Annals of Nuclear Energy 175 (2022) 109193

Contents lists available at ScienceDirect

Annals of Nuclear Energy

journal homepage: www.elsevier.com/locate/anucene

Signal processing applied in cortex project: From noise analysis to OMA and SSA methods

C. Montalvo [a,*], L. Pantera [b], S. Lipcsei [c], L.A. Torres [a]

[a] Energy and Fuels Department, Universidad Politécnica de Madrid, Ríos Rosas 21, 28003 Madrid, Spain
[b] CEA, DES, IRESNE, DER, SPESI, LP2E, Cadarache, 13108 Saint-Paul-Lez-Durance, France
[c] Centre for Energy Research, P.O. Box 49, Budapest H-1525, Hungary

ARTICLE INFO

Article history:
Received 17 January 2022
Received in revised form 28 April 2022
Accepted 2 May 2022
Available online 24 May 2022

Keywords:
SSA
Neutron noise
KWU
VVER
Signal processing
OMA

ABSTRACT

In the framework of the CORTEX EU project, several measurements from different KWU and VVER reactors have been analyzed. The goal of this project is to develop and test core monitoring techniques to detect possible anomalies and better characterize the information provided by the neutron detectors. In this article, three different signal processing methods are presented: coolant velocity estimation, Singular Spectrum Analysis (SSA) and Operational Modal Analysis (OMA). The first method is based on detecting travelling perturbations by cross correlating different detectors and obtaining the impulse response function. The second method, SSA, reduces the noise and allows a better estimation of the frequency content with a high resolution. SSA has been tested both in simulated and plant data. The last method permits distinguishing closely spaced resonances and a multivariate analysis of all the detectors. In this work, the details of each methodology are explained step by step, and the results on each reactor are also presented. Testing these methods during CORTEX project gives valuable information and orientation for further investigations in reactors diagnostics.

1. Introduction

Neutron noise is referred as the fluctuations around the trend value which are registered by the neutron detectors (Hashemian, 2009). The processing and characterization of this noise is normally regarded as noise analysis which has been extensively used for core monitoring and diagnostics purposes in many reactors in the last decades (Hashemian, 2009, Montalvo et al., 2016, Pázsit et al., 2017, Pázsit et al., 2019, Runkel, 1987, Torres et al., 2019).

The use of noise analysis and signal processing in nuclear power plants has been applied to sensor dynamics monitoring (Montalvo et al., 2014), vibration monitoring (Pázsit et al., 2016), process control (Hashemian, 2011), etc. There are many examples of these applications in the literature over the years (Pázsit et al., 2017, Pázsit et al., 2014).

In 2017, the European project CORTEX (CORe monitoring Techniques: EXperimental validation and demonstration) began with the objective of developing and testing innovative core monitoring techniques that allow to detect anomalies in nuclear reactors, such as excessive vibrations of core internals, flow blockage, coolant inlet perturbations, etc (Demazière, 2020). Over 60% of the current fleet of nuclear reactors is composed of units that are more than 30 years old (Demazière, 2020), so early detection of anomalies is crucial.

From the point of view of signal processing, nuclear power plants operate normally in steady state conditions, that is, no transients or sudden changes are observed. So, it is important for monitoring tools to be able to distinguish normal fluctuations from abnormal fluctuations. This implies to characterize in detail all the information registered by the detectors and in this special case, by the neutron detectors.

One of the challenges of signal processing in the last years was developing tools that could filter and decompose the signals in different frequency bands (Amplitude, Frequency Time methods). Some examples of these methods applied in nuclear reactors are Short Time Fourier Transform (STFT) (Montalvo et al., 2017), Hilbert-Huang Transform (HHT) (Prieto-Guerrero and Espinosa-Paredes, 2014, Blázquez et al., 2013) and Wavelet transforms (Tagaris et al., 2019). In all cases, these methods have been used in situations where there was a transient. Nevertheless, its use in steady state conditions does not improve the capabilities of standard Fourier based methods.

The processes that take place in a reactor are a consequence of different physical phenomena (Bermejo, 2014, Seidl et al., 2015), such as mechanical vibrations or thermalhydraulic processes,

* Corresponding author.
E-mail address: cristina.montalvo@upm.es (C. Montalvo).

https://doi.org/10.1016/j.anucene.2022.109193
0306-4549/

which affect the detectors response. Therefore, it is very important for signal processing techniques and monitoring tools to be able to differentiate which phenomenon is responsible for the different characteristics of the signals. These phenomena can overlap in the same frequency range, so filtering in different frequency bands is not useful for this.

The monitoring techniques need to distinguish different sources of perturbation in the same or different frequency ranges as well as isolate those perturbations which may be transporting along the core. For that purpose, in this work the authors propose to use three different methods that have been developed and tested in real plant data during the CORTEX project.

The first method is Fourier based and it is meant to detect the transit time of travelling perturbations in the core. The second method, Singular Spectral Analysis (SSA), is able to extract relevant frequencies with higher resolution based on a decomposition performed in the time domain. The last method, Operational Modal Analysis (OMA), distinguishes different phenomena in the signals and in the same frequency range by decomposing the spectra in the frequency domain. All the methods have been tested in plant data from KWU reactors and VVER reactors in different cycles. The details of each methodology are explained step by step, and the results on each reactor are also presented. Testing these methods during CORTEX project gives valuable information and orientation for further investigations in reactors diagnostics. The results presented are an overview of the possibilities of these techniques and their utility for core monitoring.

2. Data analyzed from cortex project and overview of methods developed

The work presented in this article takes place in the framework of the EC H2020 European CORTEX project (The European CORTEX project, 2018). The project aims at developing innovative core monitoring techniques that allow to detect anomalies in nuclear reactors during operation using the perturbated neutron flux measurements (so-called Neutron Noise) recorded by the in-core and ex-core instrumentation. One of the goals of the project is to improve/develop signal processing methods for a better characterization of the neutron detectors data. The applied techniques are first tested on signals generated by a simulated process mimicking specific anomalies such as vibrating central cluster of fuel assemblies or fluctuations of inlet coolant flow. Then actual data are used to test the methods developed within the project.

Several partners within the CORTEX consortium have provided data. In this paper, the data belongs to a three-loop KWU reactor, a four-loop KWU reactor, a VVER-440 reactor and a VVER-1000 reactor.

In the following subsections, the set of measurements analyzed, and the core layout of every reactor are described.

2.1. KWU reactors

These reactors have eight ex-core detectors and between 36 and 48 in-core detectors. In the three-loop reactor, the in-core detectors are located in six radial positions (G2, J6, N8, J14, G10 and C8) and at six axial levels (S1-S6) as can be seen in Fig. 1, that makes a total of 36 in-core detectors. In the four-loop reactor, the in-core detectors are located in eight radial positions and at six axial levels. This makes a total of 48 in-core detectors for this case as can be seen in Fig. 2.

The total data analyzed for the KWU reactors is shown in Table 1:

2.2. VVER reactors

The VVER-440 reactor layout is presented in Fig. 3 where the locations of the in-core detectors (SPND, Self Powered Neutron Detector) are also specified.

In the case of the VVER-440, the data analyzed consists of three measurements from the same fuel cycle of Unit 2. The details are in Table 2.

The core layout of the VVER-1000 reactor is presented in Fig. 4 where the radial location of in-core detectors, ex-core detectors and accelerometers is indicated.

The axial location of the detectors is shown in Fig. 5.

The data analyzed in this reactor covers up to four consecutive cycles as can be seen in Table 3.

2.3. Methods developed within the project

As previously mentioned in the article, one of the goals of CORTEX project is improving the signal processing techniques to better characterize the neutron detectors data and therefore, differentiate the different phenomena which takes place in the reactor. This is especially difficult when the data is stationary and no transients are observed and, that is what happens in normal operation conditions. The standard noise analysis techniques are very useful for dealing with stationary data but they are not able to achieve certain goals proposed in CORTEX such as:

- Monitoring the velocity of travelling perturbations by decomposing the signal into local and global components.
- Decomposing the signals in the time domain in different parts based on their frequency content. These different parts can be linked to different physical processes.
- Detrending the signals.
- Decomposing the signals in the frequency domain and differentiate dominant phenomena from other processes less relevant in the reactors within the same frequency range.
- Characterize in detail closely spaced resonances.
- A multivariate analysis that gather all the information from all the detectors.

The article is organized as follows:

- **Section 3** covers all the aspects related to the **coolant velocity estimation method**. This method focuses on detecting travelling perturbations by improving the standard cross correlation technique between distant detectors.
- **Section 4** explains the possibilities of **SSA methodology** which allows decomposing the signals in the time domain, reducing the noise in the spectral analysis and consequently, improving the estimation of the principal characteristic frequencies is achieved with a higher resolution.
- **Section 5** deals with the **OMA** based methods which are able to distinguish closely spaced resonances and to decompose the spectra in different parts that can be linked to different physical phenomena. Besides, the technique provides a multivariate analysis that include all the detectors in the reactor.

3. Coolant velocity measurement in VVER-440 reactors

Like other power reactors, there is no instrumentation installed in VVER-440 reactors for measuring coolant velocities in the reactor core, only their average value is estimated using the total mass flow rate. However, the fluctuating part of the SPND signals carries information of propagating perturbations traveling with the coolant, and thus the coolant velocity can be estimated with a correla-

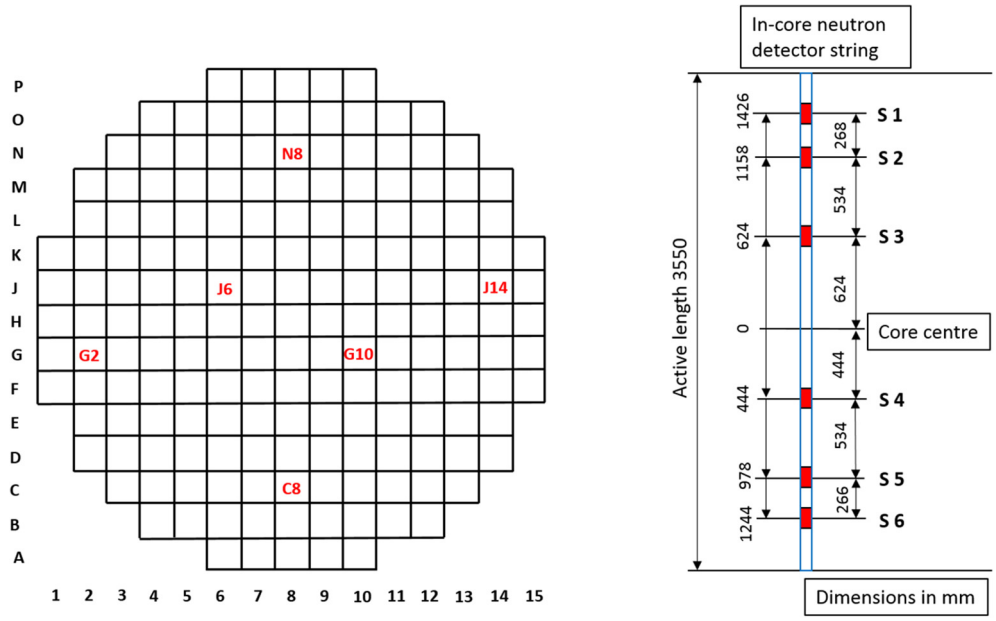

Fig. 1. Generic layout of the location of the in-core detectors in the three-loop KWU reactor.

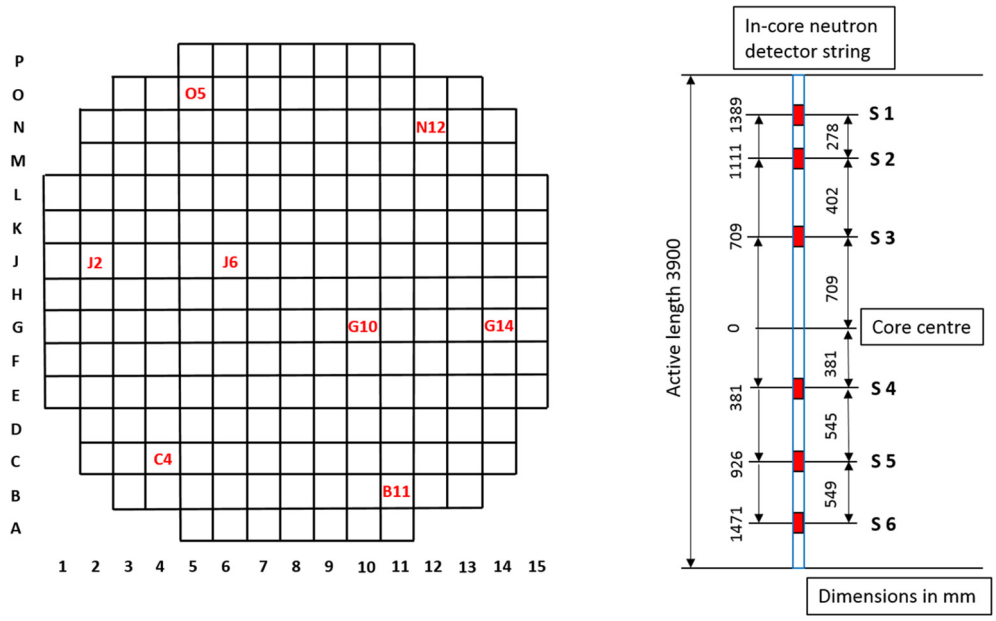

Fig. 2. Generic layout of the location of the in-core detectors in the four-loop KWU reactor.

Table 1
Sets of measurements analyzed in KWU reactors. BOC, MOC and EOC stand for beginning, middle and end of cycle.

REACTOR	Measurement 1	Measurement 2	Measurement 3	Measurement 4
3 LOOP	Cycle 39 (MOC39)	Cycle 39 (EOC39)	Cycle 40 (BOC40)	Cycle 40 (MOC40)
4 LOOP	M.30 (27 03 2012)	M.31 (12 06 2013)	M.32 (17 04 2014)	

tion method in the fuel assemblies equipped with neutron detector chains (Adorján et al., 2000).

3.1. Basic principle of the method

A perturbation moving along two detectors causes small transients in the detector signals with a time delay proportional to the distance between the detectors (Fig. 6). The time delay – which can directly be identified in the time series of the signals in an ideal case – can generally be read from the cross-correlation function $CORR_{12}(\tau)$ having a local maximum at the time delay.

$$CORR_{12}(\tau) = \lim_{T\to\infty} \frac{1}{T} \int_{-\frac{T}{2}}^{\frac{T}{2}} \delta i_1(t)\delta i_2(t-\tau)dt \quad (1)$$

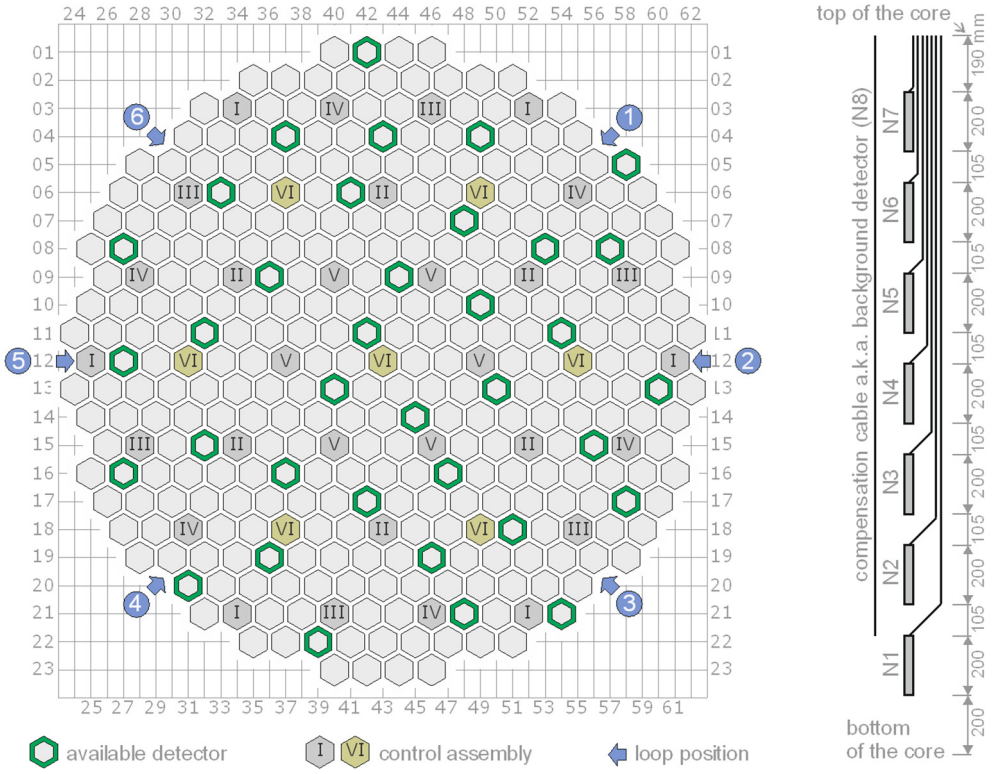

Fig. 3. Core layout of the VVER-440 reactor and radial and axial location of in-core detectors.

Table 2
Data analyzed from VVER-440.

	BOC	MOC	EOC
Measurement date	2017–01-03	2017–05-26	2017–11-29
EFPD [days]	7.96	149.73	335.13

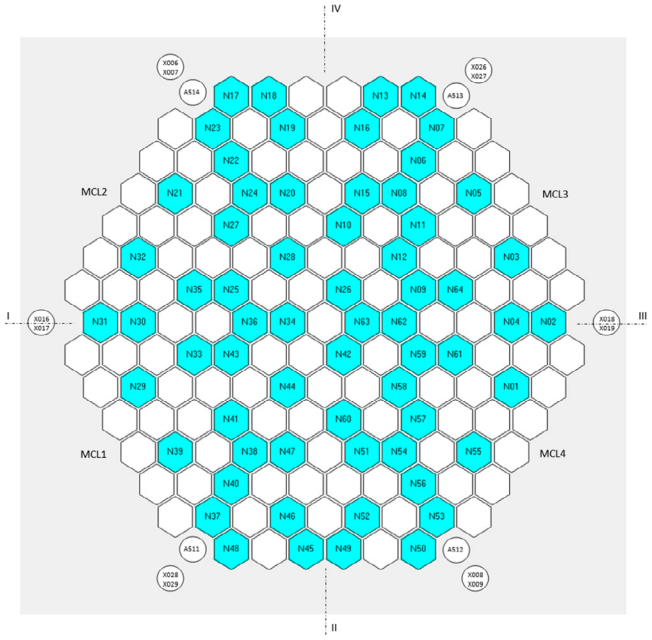

Fig. 4. Height radial locations of in-core (N…), ex-core (X…) neutrons detectors and accelerometers (A…).

where $\delta i_1(t)$ and $\delta i_2(t-\tau)$ stand for the fluctuating content of the detector signals and τ is the correlation time.

Due to the noisy environment, separation or suppression of the disturbing signal components is necessary with frequency domain (Fourier) analysis. The Fourier transform of the detector current is:

$$\delta I(\omega) = \int_{-\infty}^{\infty} \delta i(t) e^{-i\omega t} dt,$$

and the cross-correlation function between positions z_1 and z_2 is estimated with the inverse Fourier transform of the cross spectrum:

$$CORR_{12}(t) = \frac{1}{2\pi} \int_{-\infty}^{\infty} CPSD_{12}(\omega) e^{i\omega t} d\omega, \tag{2}$$

where $CPSD_{12}(\omega) = \left\langle \delta I_1(\omega), \delta I_2(\omega) \right\rangle$. The transfer function,

$$H(\omega) = \frac{CPSD_{12}(\omega)}{APSD_1(\omega)}.$$

between the two signals is free from the transfer properties of the measurement chains since both spectra of the above quotient contain them. Its inverse Fourier transform estimates the impulse response function,

$$IMP_{12}(t) = FFT^{-1}(H(\omega)) = \frac{1}{2\pi} \int_{-\infty}^{\infty} \frac{CPSD_{12}(\omega)}{APSD_1(\omega)} e^{i\omega t} d\omega. \tag{3}$$

This function shows a more definite peak at the time delay in comparison with the correlation function.

A more detailed explanation and some improvement of the method can be read in (Kiss and Lipcsei, 2022).

3.2. Measurement in the reactor core with SPNDs

The detectors of the reactor core measure not only the propagating perturbation $\delta I^{(T)}(\omega)$, but a strongly correlated $\delta I_\phi(\omega)$ back-

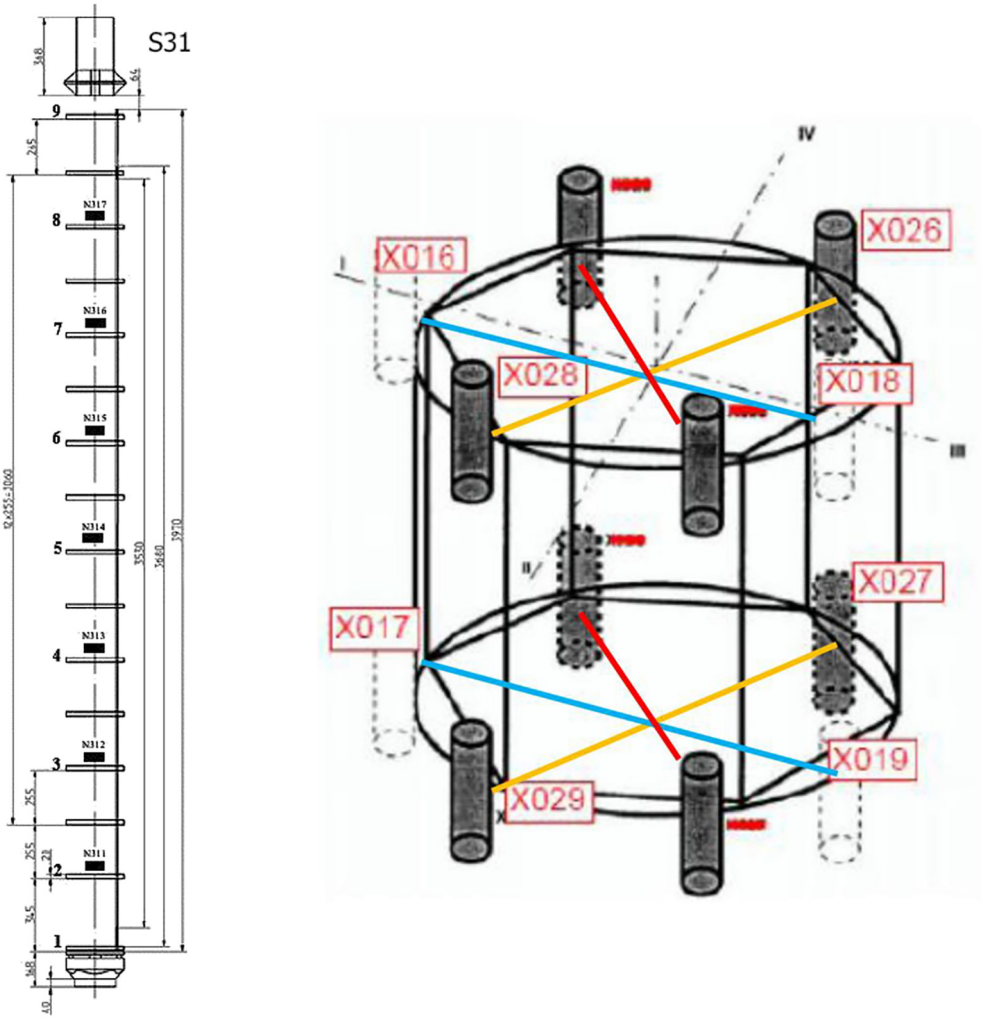

Fig. 5. Axial locations of in-core (N...) and ex-core (X...) neutrons detectors in VVER-1000.

Table 3
Data analysed from VVER-1000.

Cycle	U1C09	U1C10	U1C11	U1C12
Measurement date	2010–10-18	2011–09-21	2012–09-23	2013–09-23

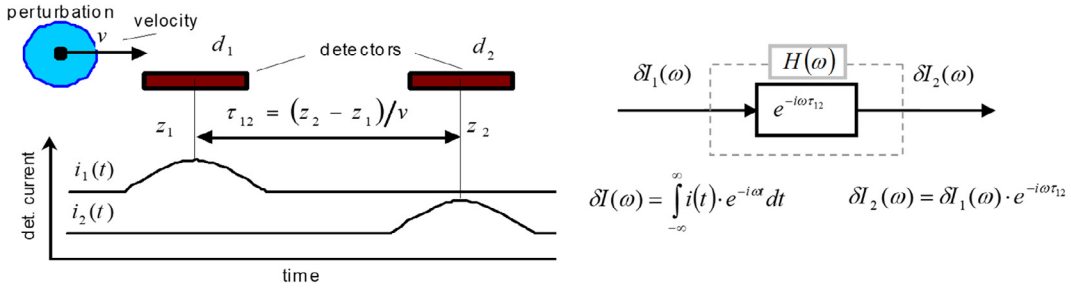

Fig. 6. Effect of a perturbation on the detector signals in the time domain (left) and the transfer function describing the phenomenon in the frequency domain (right).

ground noise which can be sensed permanently at any point of the core and disturbing $\delta W(\omega)$ noise signals as well. These noise sources are marked in the left side of Fig. 7 showing the coolant flow in the pressure vessel of a VVER-440 reactor. $H(\omega)$ is the transfer function between the positions z_1 and z_2 consisting of the factor $e^{-i\omega\tau_{12}}$ describing the propagating perturbation (where $\tau_{12} = (z_2 - z_1)/v$ denotes the transit time between the two detectors), while $\widehat{H}(\omega, z)$ stands for the transfer function describing the effect of the reactor core on propagating perturbations depending on location (Fig. 7). Such effects can e.g., be the increase of the

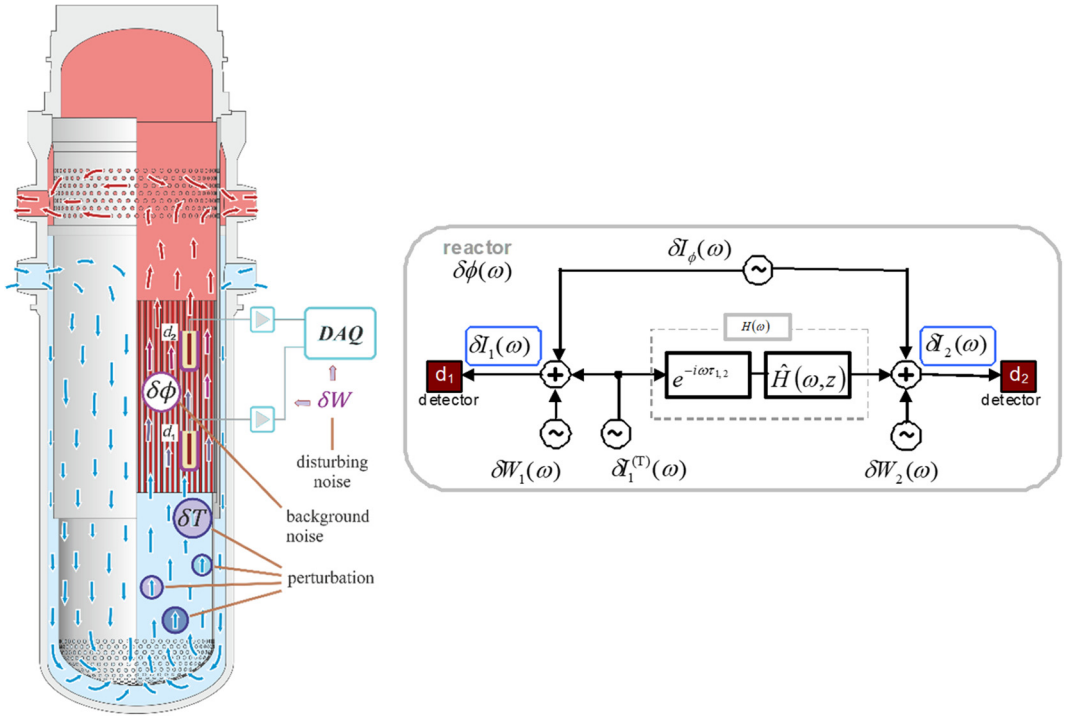

Fig. 7. Pressure vessel of a VVER-440 reactor with the coolant flow and noise sources (left) and scheme of the propagating of perturbations along two detectors in the core (right).

coolant velocity due to heat expansion or the change of the shape of the neutron flux or the change of the size of the perturbation. These effects are generally neglected during the velocity estimation i.e. $\widehat{H}(\omega,z)$ is considered as constant 1 and so the transfer function is:

$$H(\omega)=\widehat{H}(\omega,z)e^{-i\omega\tau_{12}}\approx e^{-i\omega\tau_{12}}.$$

Based on the right-hand-side scheme of Fig. 7, the fluctuation of the current induced by a propagating perturbation in the detector at position z_1 and z_2 can be written as:

$$\delta I_1(\omega)=\delta I_1^{(T)}(\omega)+\delta I_\phi(\omega)+\delta W_1(\omega),$$

$$\delta I_2(\omega)=H(\omega)\delta I_1^{(T)}(\omega)+\delta I_\phi(\omega)+\delta W_2(\omega). \quad (4)$$

Let us substitute (4) into (2) and (3). Assuming that the $\delta W_i(\omega)$, $i=1,2$ terms are independent disturbing noises, then $\left\langle \delta I_1^T(\omega),\overline{\delta W_i(\omega)}\right\rangle=0$, and $\left\langle \delta I_\phi(\omega),\overline{\delta W_i(\omega)}\right\rangle=0$. Moreover, for an ideal measurement $\left\langle \delta W_1(\omega),\overline{\delta W_2(\omega)}\right\rangle=0$ as well. It is not zero e.g., when there is an undesired crosstalk between the channels of the measurement system or if some technological noises occur. Let us use the following notations: $APSD_1^{(lo)}(\omega)=\left\langle \delta I_1^{(T)}(\omega),\overline{\delta I_1^{(T)}(\omega)}\right\rangle$ is the auto spectrum of the local fluctuation caused by the propagating perturbation at a position z_1; $APSD^{(bg)}(\omega)=\left\langle \delta I_\phi(\omega),\overline{\delta I_\phi(\omega)}\right\rangle$ is the auto spectrum of the background (global) noise; $APSD_1^{(W)}(\omega)=\left\langle \delta W_1(\omega),\overline{\delta W_1(\omega)}\right\rangle$ is the auto spectrum of the disturbing noise at a position z_1; $CPSD_{1\phi}^{(gl)}(\omega)=\left\langle \delta I_1^{(T)}(\omega),\overline{\delta I_\phi(\omega)}\right\rangle$ is the cross spectrum between the local and the background fluctuations; $CPSD_{12}^{(W)}(\omega)=\left\langle \delta W_1(\omega),\overline{\delta W_2(\omega)}\right\rangle$ is the cross spectrum between the disturbing noises of the detectors, ideally it is zero. Although the propagating perturbations have contribution to the background noise, $\left|CPSD_{1\phi}^{(gl)}(\omega)\right|\ll APSD^{(bg)}(\omega)$. Assuming a good quality measurement system $APSD_1^{(W)}(\omega)\ll APSD^{(bg)}(\omega)$ and $CPSD_{12}^{(W)}(\omega)\cong 0$. Finally, with these assumptions and notations (for more details see (Kiss and Lipcsei, 2019)):

$$CORR_{12}(t)=\frac{1}{2\pi}\int_{-\infty}^{\infty}\left(H(\omega)APSD_1^{(lo)}(\omega)+APSD^{(bg)}(\omega)\right)e^{i\omega t}d\omega \quad (5)$$

The impulse response function can be originated similarly to the above:

$$IMP_{12}(t)=\frac{1}{2\pi}\int_{-\infty}^{\infty}\frac{APSD_1^{(lo)}(\omega)e^{i\omega(t-\tau_{12})}d\omega}{APSD_1^{(lo)}(\omega)+APSD^{(bg)}(\omega)}+\frac{1}{2\pi}\int_{-\infty}^{\infty}\frac{APSD^{(bg)}(\omega)e^{-i\omega t}d\omega}{APSD_1^{(lo)}(\omega)+APSD^{(bg)}(\omega)} \quad (6)$$

This sum has two local extremes. One at the τ_{12} transit time of the propagating perturbations and the other at 0 s caused by the global background noise. When the background noise is much lower than the local term ($APSD^{(bg)}(\omega)\ll APSD_1^{(lo)}(\omega)$), the first term of the sum dominates and causes a sharp peak at τ_{12}. Otherwise, when the background is much larger than the local term ($APSD^{(bg)}(\omega)\gg APSD_1^{(lo)}(\omega)$), the second term of the sum causes a sharp peak at 0 s. Since $APSD^{(bg)}(\omega)$ and $APSD_1^{(lo)}(\omega)$ both have similar frequency dependence (they are characterized by the $\frac{1}{k^2+\omega^2}$ like decreasing shape of the neutron noise spectra above 1.5 Hz), both peaks can be identified in most of the situations.

Some typical cross correlation and impulse response functions are presented in Fig. 8 between detectors at the top (level 7) and the bottom (level 1) of the reactor core.

Fig. 8 demonstrates that the impulse response function separates the peak of the global background noise at 0 s from the peak at the transit time of the propagating perturbation much better than the correlation function. Such functions often contain much more disturbances than the functions provided in the figure: here we have selected the ones that best show the effect. For these

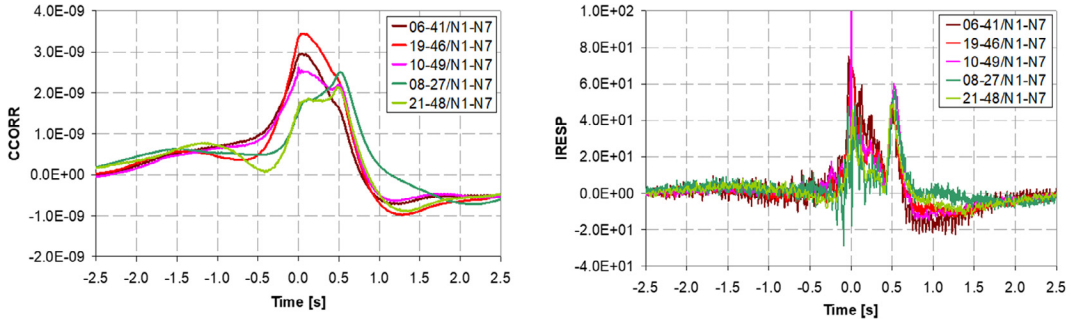

Fig. 8. Cross correlation (left) and impulse response functions (right) with different background noises.

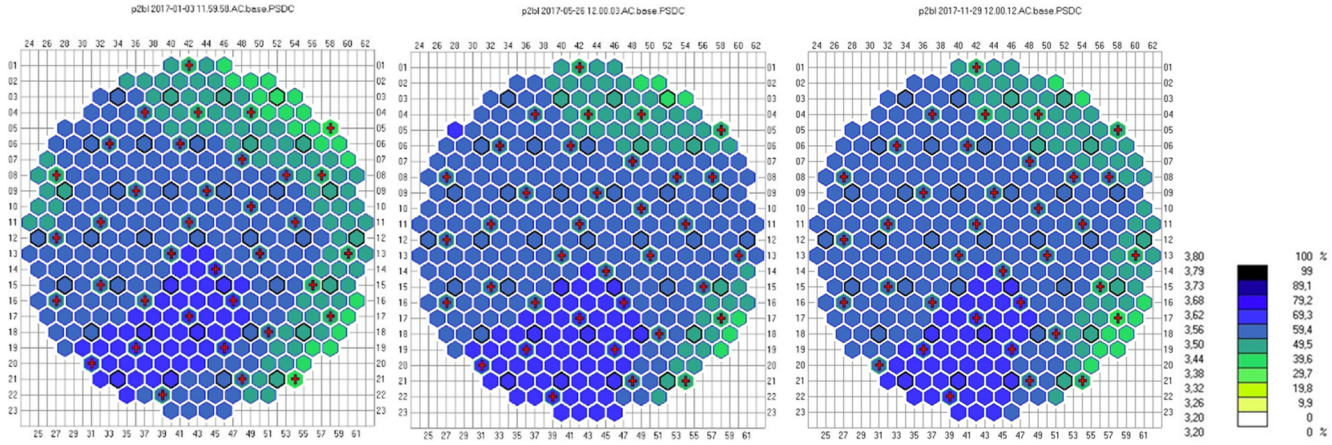

Figure 9: Radial distributions of the coolant velocities

Fig. 9. Radial distributions of the coolant velocities.

graphs, the two farthest detectors of the chains are used, because they provide the smallest relative error. Additionally, the uppermost detector has the shortest cable and so the smallest disturbing effect of the cable signal, while the global background noise can be partly compensated by the cable signal of the bottommost detector (due to the opposite sign of the signals of the cable and the detector).

3.3. Measurements and signal processing

Three measurements of the same fuel cycle (#32) of Unit 2 of Paks NPP were used to demonstrate the method, at the beginning (at 8 EFPD – effective full power days), at the middle (150 EFPD) and at the end (335 EFPD) of the fuel cycle. Each measurement was 1-hour-long. Stationary (DC) and fluctuating parts (AC) of the signals were produced through filters (DC: 0.4 Hz low pass; AC: 0.03 Hz high pass, 40 Hz low pass, 50 Hz notch) and measured separately with sampling frequencies of 100 Hz (AC) and 3.125 Hz (DC).

The signals were normalized with their DC values similarly to the normalization used in Western type reactors. However, the detectors are uncompensated, i.e. the detector cable distorts the DC value since the cable axially integrates the neutron flux above the detector what results an error up to 3% depending on the sensitivity of the cable and this error is neglected. When the fluctuating part of the signals is evaluated, it needs to be considered that only 6% of the Rh SPND signals is prompt in steady state.

Fourier transform of the signals were made with 4096 width Hanning windows and 50% overlapping resulting the frequency resolution of 0.0244 Hz. However, the accuracy of the transit time is determined by the resolution of the impulse response function which is equal to the sampling time of the measurement.

3.4. Results

In principle, any two detectors of the chain can be used to evaluate the transit time (and the coolant velocity) but detectors farther apart provide the highest accuracy (due to the given resolution). However, the distance between detectors cannot be too large, since the correlation between the detector signals

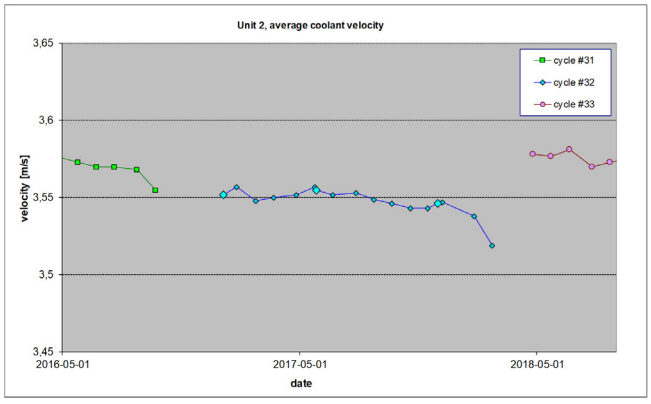

Fig. 10. Average coolant velocities in the trend of regular velocity measurements.

decreases with the distance which results in a deterioration in the readability of transit time. The optimal distance is determined empirically for the given measurement arrangement.

For VVER-440 reactors, detector pairs 1–5 and 2–6 provide the best results, graphs in this section have been calculated with them. In practice, pairs 1–4, 1–5, 1–6, 2–5, 2–6, 3–6 are still usable, the result can be further improved with the weighted average of the transit time determined using these detector pairs (Adorján et al., 2000).

Radial distributions of the fuel assembly average coolant velocities are shown in Fig. 9 for the three measurements. The smooth graphs refer to a still operation over the fuel cycle.

These kinds of evaluations are performed in a regular base in the reactor units of the Paks NPP. Core average values of the present evaluations are displayed with bigger markers in the trend of the regular measurements in Fig. 10 as a validation of the three measurements provided for the Cortex project. The new values well fit in the trend which have a change of less than 0.5% during the fuel cycle.

4. Singular spectral analysis applied to the VVER-1000 measurements

In the context of the processing of Acoustic Emission Signals acquired in the framework of the experimental campaigns at the CABRI facility (French nuclear research reactor) (Pantera and Traore, 2015) we use classical methodologies (Traore et al., 2017b, Traore et al., 2016) to pre-process the data. Such methods have proven to be very robust on our noisy data. We consider them as reference methods against which alternate methods can be tested, in particular to see if it would be possible to extract more information from our data. The Singular Spectrum Analysis (SSA) is one of those alternate methods, which has received increasing attention since the early nineties. Unlike most methods for time series analysis, SSA needs no statistical assumption on signal or noise. By using a decomposition of the signal into the sum of a small number of independent and interpretable components, SSA allows to perform various tasks such as extraction of specific components from a complex signal (noise, trend, seasonality ...), detection of structural changes and missing values imputation. We have explored the ability of the SSA to analyze and denoise the Acoustic Emission (AE) signals (Traore et al., 2017a). We try here to use this approach on neutron noise data. Firstly, we will apply the method to simulated data in order to understand how it works. Then we will apply it to actual power plant data in order to highlight how this method could be applied to improve the classical approaches. In this study, we merely adopt an exploratory approach for every sensors. We will show how the SSA method can reduce the noise in the spectral analysis allowing us to estimate the principal characteristic frequencies with a higher resolution. From a technical point of view, when we use the SSA terminology we imply Basic SSA. In the cases where it can be assumed that the signal is stationary, it would be possible to enhance the results with the use of a Toeplitz SSA (cf. (Golyandina et al., 2001) for more details). We do not perform a physical analysis of the results from all the sensors in order, for instance, to correlate events in the core and the calculated frequencies. Such a study will be the subject of another survey.

4.1. Principle of the SSA method

Consider a real-valued non-zero time series $(x_1, \cdots, x_n)$ of length N. The main purpose of SSA is to decompose this time series into a sum of a small number of independent time series representing components of interest and residual. The SSA technique consists of two complementary stages: decomposition and reconstruction. In this section, we briefly summarize the different steps, for further details on theoretical aspects we report the reader to references (Golyandina et al., 2001,Hassani, 2007).

4.1.1. Decomposition stage

The decomposition stage is divided into embedding and singular value decomposition.

4.2. Embedding

Embedding is a classical procedure in time series analysis (Broomhead et al., 2020, Kantz and Schreiber, 2004). It can be considered as a mapping which transfers the one-dimensional signal into the multidimensional signals $X_1, \cdots, X_k$ where $X_i = (x_i, \cdots, x_{i+L-1})^T \in \mathbb{R}^L$ and $K = N - L + 1$. The vectors, called L-lagged vectors, are grouped into the trajectory matrix.

$$X = [X_1, \cdots, X_k] = \begin{pmatrix} x_1 & x_2 & \cdots & x_k \\ x_2 & x_3 & \cdots & x_{k+1} \\ \vdots & \vdots & \vdots & \vdots \\ x_L & x_{L+1} & \cdots & x_N \end{pmatrix}$$

This matrix being a Hankel matrix, all the elements along the diagonal $i + j = const$ are thus equal. The single parameter of the embedding step is the window length L which is an integer such that $2 \leq L \leq N$. The SSA technique explores the empirical distribution of the pairwise distances between the lagged vectors X_i and X_j. So the choice of the dimension L of the lagged vectors is of major importance in SSA implementation, since it determines the quality of the decomposition.

4.3. Singular value decomposition (SVD)

Based on the so-called SVD theorem, the second step of the decomposition stage consists in applying a SVD of the trajectory matrix. Denote by $\lambda_1, \cdots, \lambda_N$ the eigenvalues of the matrix XX^T following the decreasing order of magnitude $(\lambda_1 \geq \lambda_2 \geq \cdots \geq \lambda_L \geq 0)$, and by $U_1, \cdots, U_L$ the orthonormal system of the associated eigenvectors. Let $= max\{i\, such\, that\, \lambda_i \geq 0\}$. If we consider $V_i = \frac{X^T U_i}{\sqrt{\lambda_i}}$ the SVD of the trajectory matrix X can be then represented as a sum of rank-one bi-orthogonal elementary matrices $X_i = \sqrt{\lambda_i} U_i V_i^T$:. $X = X_1 + \cdots + X_d$

The collection (λ_i, U_i, V_i) is called the eigentriple of the SVD.

4.3.1. Reconstruction stage

The reconstruction stage is composed of two parts: grouping and selection of the groups for the reconstruction.

4.4. Grouping

The grouping procedure consists in partitioning the set of indices $\{1 \cdots d\}$ into several groups, and in summing the matrices within each group. Considering the group $I = \{i_1, \cdots, i_p\}$ and the associated matrix X defined as $X_I = X_{i_1}, \cdots, X_{i_p}$ the split of the set of indices $\{I_1, \cdots, I_m\}$ leads to the decomposition:. $X = X_{I_1} + \cdots + X_{I_m}$

The procedure for choosing the set $\{I_1, \cdots, I_m\}$ is called the eigentriple grouping. This procedure is not very formal. Each group is entended to represent an additive component of the time series (trend, oscillatory component, noise). We will elaborate our method in section 4.3.3.

4.5. Groups selection for the reconstruction

In the grouping summation, we can remove some groups related to the components we are not interested in according to the analysis objectives.

4.6. Application of SSA in simulated data

We use simulated data provided in (Dokhane and Mylonakis, 2018). In order to generate the desired data, models for in-core and ex-core detectors have been developed using the Simulate 3 K code (S3K) for the four-loop Westinghouse PWR mixed core of the OECD/NEA transient benchmark (Chionis et al., 2018). We chose in the scenario 5 the data relative to the 5x5 central Fuel Assembly (FA) cluster undergoes a sine wave vibration of 1 mm and frequency of 1.5 Hz in horizontal direction. In this section, we worked only on one signal. It was meant for testing SSA on a signal whose frequency content is known.

The simulation has a duration of 100 s and a time step of 0.01 s. Hence the sampling frequency is equal to 100 Hz. Fig. 11 shows the time evolution of the simulated data and Fig. 12 its frequency content.

We will apply now the SSA method on this data. We gather in Fig. 13 the results of the analysis.

4.6.1. SSA analysis: Decomposition stage

The upper left graph in Fig. 13 confirms that the signal is contained principally in the first eigentriple since the two corresponding eigenvalues are larger than the residual components eigenvalues. There is also a part in the 3–6 eigentriples which seems not to be in the residual part.

The lower left graph in Fig. 13 shows that the pairs 1–2, 3–4, 5–6 are produced by sin waves and the pairs 7–8, 9–10, 11–12 by a modulated sine waves. We can see on the upper right graph the amplitude decreasing of the sin waves.

The interpretation is based on the fact that a sine wave produces two eigentriples, which are sine waves with the same frequency and have a phase shift exactly or approximately equal to $\pi/2$, due to the orthogonality of eigenvectors which can be seen on the upper right graph in Fig. 13.

The lower right graph shows the correlation matrix between the eigenvectors. The matrix of absolute values of w-correlations is depicted in grayscale (white color corresponds to zero and black color corresponds to the absolute values equal to 1). We can see that there is no trend component (because there is no single eigenvalue) and three pairs are clearly separated between themselves, since the w-correlations between the pairs are small, while w-correlations between the components from the same pair are very large. The block of 10–30 components is "gray," therefore we can expect that these components are mixed and are largely produced by noise.

Since we remark in this analysis that there is no trend component, the signal can be considered as a stationary signal made up of three sine waves.

4.6.2. SSA analysis: Reconstruction stage

The reconstruction step deals with the selection of some groups of components which would be able to describe the original signal deleting the noise part. According to the last section, we decide to reconstruct the signal only with the three sine waves. On a real case, the difficulty is to select the factors for the reconstruction. The choice depends on the objectives, it is not very formal. We will show a method that can help on a real case because the number of factors to explore can became very important when the spectral content of the signal is rich. We will group the factors according to their similarities. Thus, we do a classification on the factors using the correlation to define the proximity between each others. The dendrogram in Fig. 14, result of the hierarchical classification, allows us to make an idea of the existence of several groups of components judging in the same time of their proximity. We indicated by colors how we decided to cut the classification tree in order to extract eight groups. The different sine wave are well highlighted.

We can now do the calculation of the spectrum of every group (see Fig. 15) in order to describe the spectral contents of the signal. In this case, Fig. 15 shows that some classes could be characterized by a specific frequency content, giving the possibility to isolate in some subspace different frequency content in order to keep or eliminate according to the different aspect of the physical scenario we want to highlight.

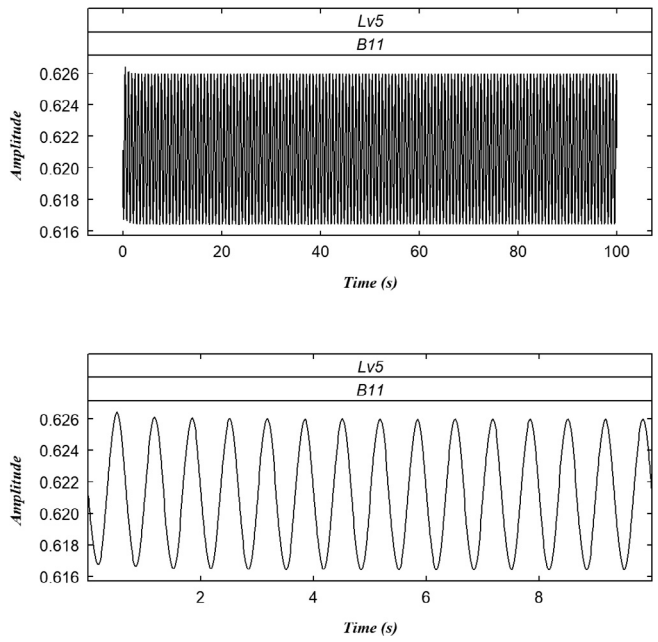

Fig. 11. Time evolution for the simulated data.

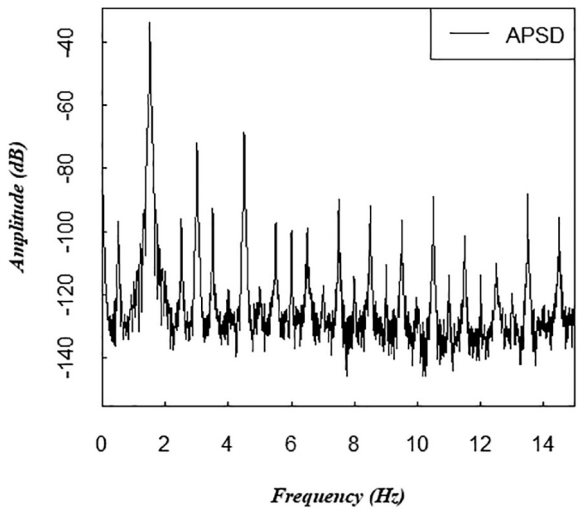

Fig. 12. Frequency content of the simulated data.

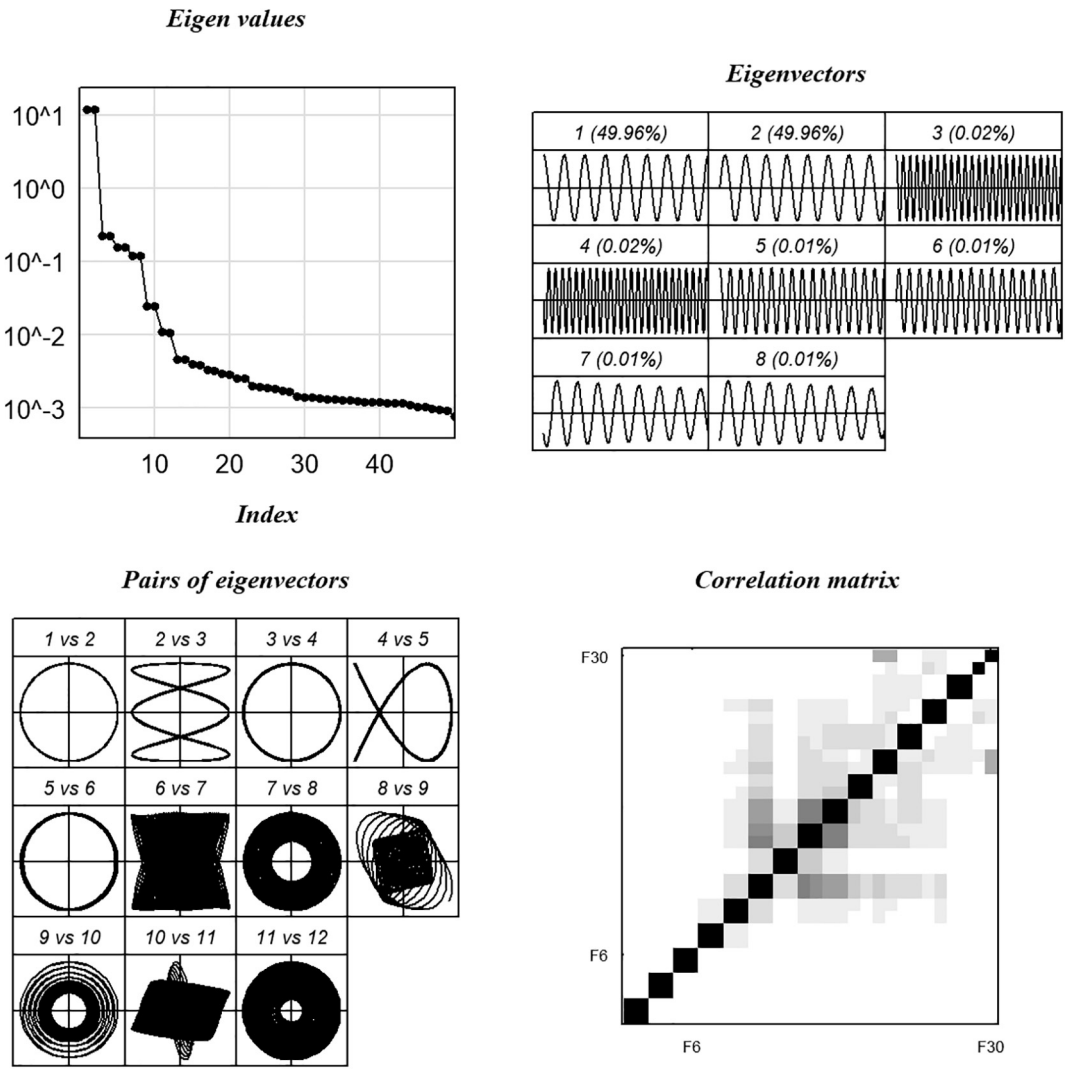

Fig. 13. Basic SSA results for the simulated data.

4.7. Application of SSA in actual plant data

In this section, we apply the method on actual plant data acquired by the in-core detectors of the Temelín VVER-1000 reactor in the Czech Republic. The real data used for this article were acquired in the framework of the study of the control rod insertion reliability. For that purpose, we had followed the migration of one assembly in the core through four consecutive fuel cycles, so-called U1C09, U1C10, U1C11 and U1C12 (Stulík et al., 2019a, Stulík, et al., 2019b). At the end of the last cycle, a problem related to an Incomplete Rod Insertion (IRI) occurred. We applied the method for all the cycles but we will show only data acquired at the beginning of the first cycle U1C09. In the framework of this article we will not discuss the IRI problem. We analyzed two types of sensors:

- Rhodium Self Power Neutron Detectors (SPND), in-core locations.
- Ionisation chambers, ex-core locations.

Fig. 4 and Fig. 5 in section 2 help us to locate the sensors according to their namings which indicate the radial and axial position. The sampling frequency is 1000 Hz and the duration is around 15 min.

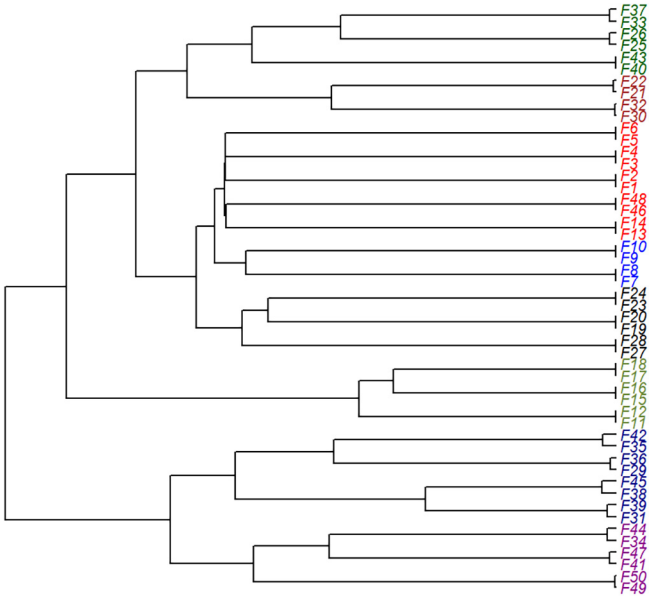

Fig. 14. Classification tree on the SSA factors.

4.7.1. Data Pre-processing

From the time evolution measurement of a neutron detector, we can show in Fig. 16 an example the Power Spectral Density on several frequency ranges:

- global: all the frequencies, from 0 to 500 Hz
- part-1: the very low frequencies
- part-2: the range between 0 and 50 Hz
- zoom-part-2: a zoom on the part-2

The global part shows us the presence of the 50 Hz frequency with its multiples that is to say 100, 150, 200, 250, 300, 350, 400 and 450 with a high energy. In part-1, the low frequencies, the power spectrum shows a 1/f spectral distribution under around 2 Hz. The duration of the cycle, around a quarter of an hour, with a sampling frequency equal to 1 kHz give us good condition to detect very low frequencies with the fast Fourier transform. Above 50 Hz, there is only one frequency, at 120 Hz, which is not multiple of 50 Hz.

Doing a Singular Spectrum Analysis on such an input signal will highlight on the first factors of these features. Indeed, the eigenvalue profile is related to the power spectrum ordered from the biggest value to the smallest one. But, finally, these features are not interesting in the study of the frequency structure in our case: the multiple of 50 Hz are pointless and we do not study the delayed neutrons. Thus, we will realise the SSA on a filtered signal. We apply a high pass filter with a cut frequency equal to 2 Hz and several stop band to remove the 50 Hz and the harmonics (cf. Fig. 17). In fact, we see that, except for the frequency at 120 Hz, the range of interest is between 2 Hz and 50 Hz. Hence, it is possible to decimate the signal by a factor of 10 without losing information (except for the frequency at 120 Hz we will not try to explain here).

4.7.2. A second pre-processing: Detrend the signals when it is necessary

In Fig. 18, we notice a trend in the in-core rhodium SPND before achieving a steady state. On the contrary, there is no trend in the ex-core sensors, that is to say the ionization chambers which are more reactive to the neutron flux detection.

In order to analyse the neutron noise, it is necessary firstly to detrend the signal acquired online. For example, in Fig. 19 we can see the presence of a trend in the sensor N315 measurement. For that purpose we can use the SSA decomposition.

Fig. 20 gives the evolution of the eigenvalues. The ideal grouping of eigenvectors is in pairs, where each pair has a similar eigenvalue, but differing phase which usually corresponds to sin-cosine-like pairs. Hence, from the shape of the leading singular

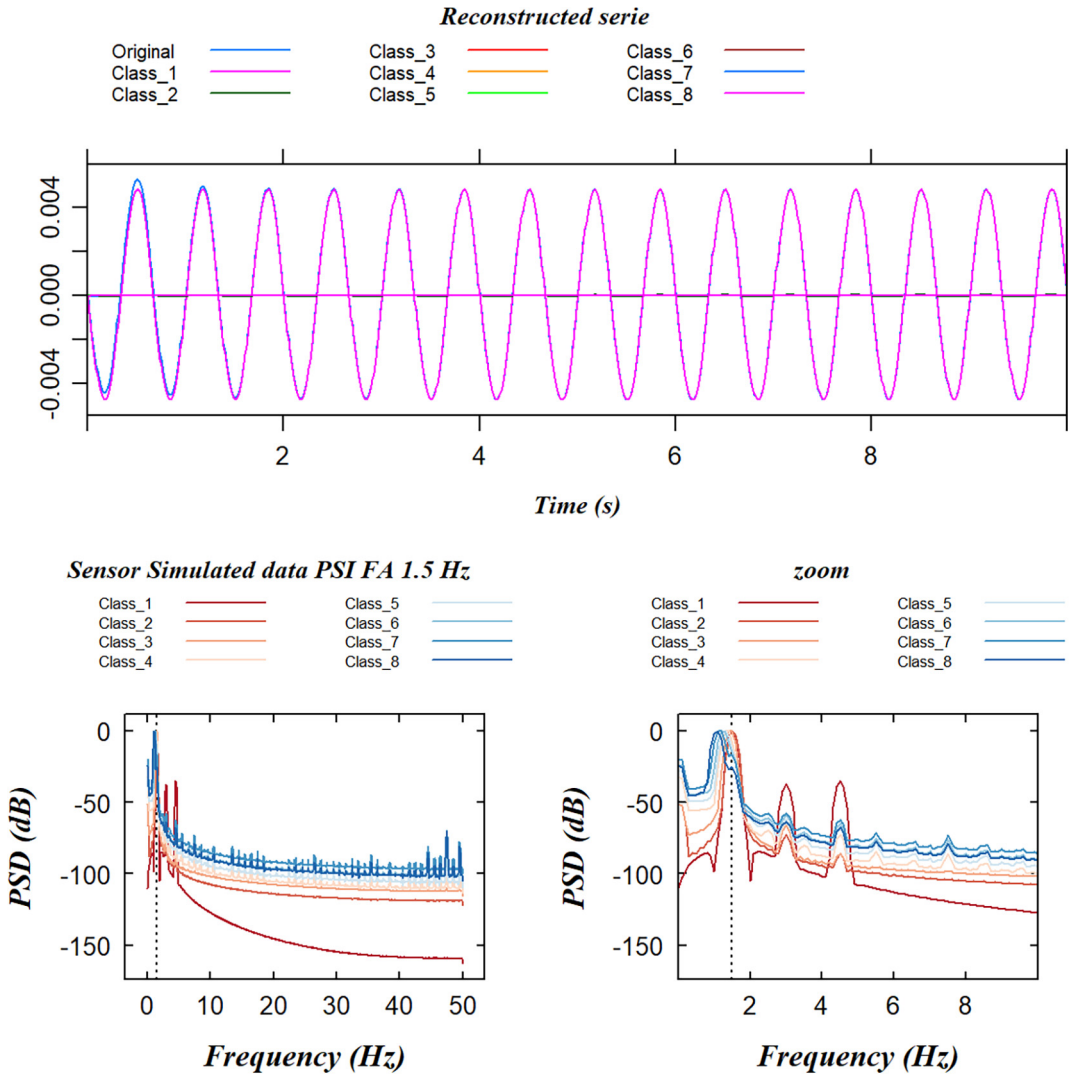

Fig. 15. Simulated data: spectrum analysis on the factors after reconstitution.

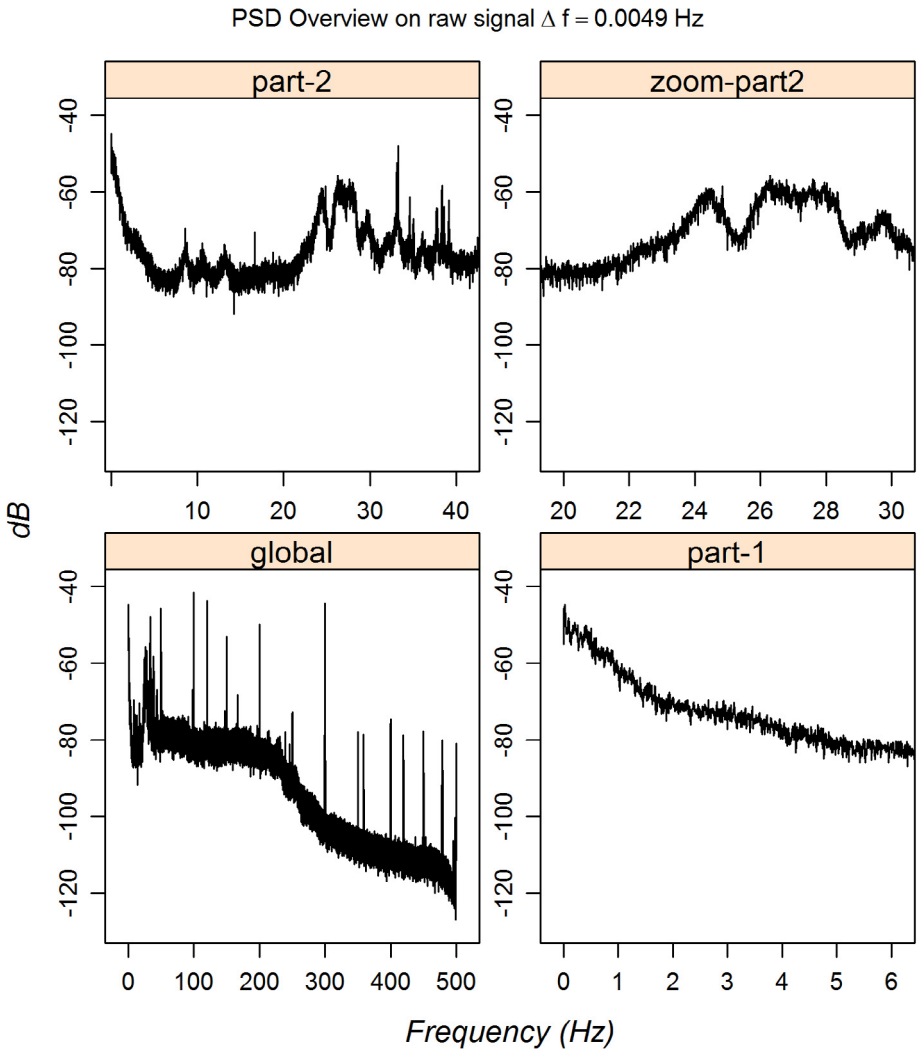

Fig. 16. PSD overview on an in-core detector raw signal.

values, we affect the first four factors, that is to say not paired values, at the trend.

In Fig. 21 we see the reconstruction using the first four factors for the trend (S1). We can visualize the result in Fig. 22 and at last, by difference between the raw data and the trend, the neutron noise estimation in Fig. 23. It is only at this stage that we can use the signal to do further analysis. We can for example transform this time evolution in an image to feed a convolutional neural network for classifying anomalies (Tagaris et al., 2019).

4.7.3. SSA analysis on the detrended signal

At this stage, we have detrended our signal and reduce the range of the spectral range to improve our analysis. We will do again the SSA approach to describe the spectral content. As expected, the leading eigenvalues (cf. Fig. 24) shows now only eigenvectors organized in pairs, there is no more trend, only oscillations. We decomposed the signal in 300 components but only 60 have been represented. Fig. 25 shows the correlation matrix which propose to keep about twenty eigen factors to reflect the maximum frequency response. In order to describe the spectral content, we first realize a classification of the components in 10 classes (we highlight only the class 3 and 10 in Fig. 26. This classification is similar to the so-called correlation clustering of variables used in multivariate statistics. We use the Ward criterion for the agglomerative algorithm. Then, the power spectrum of every class was

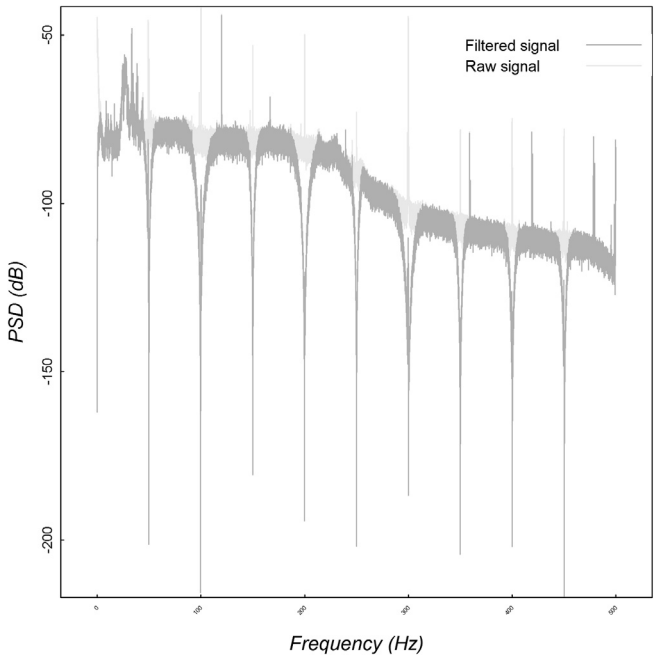

Fig. 17. The SSA is applied on the filtered signal.

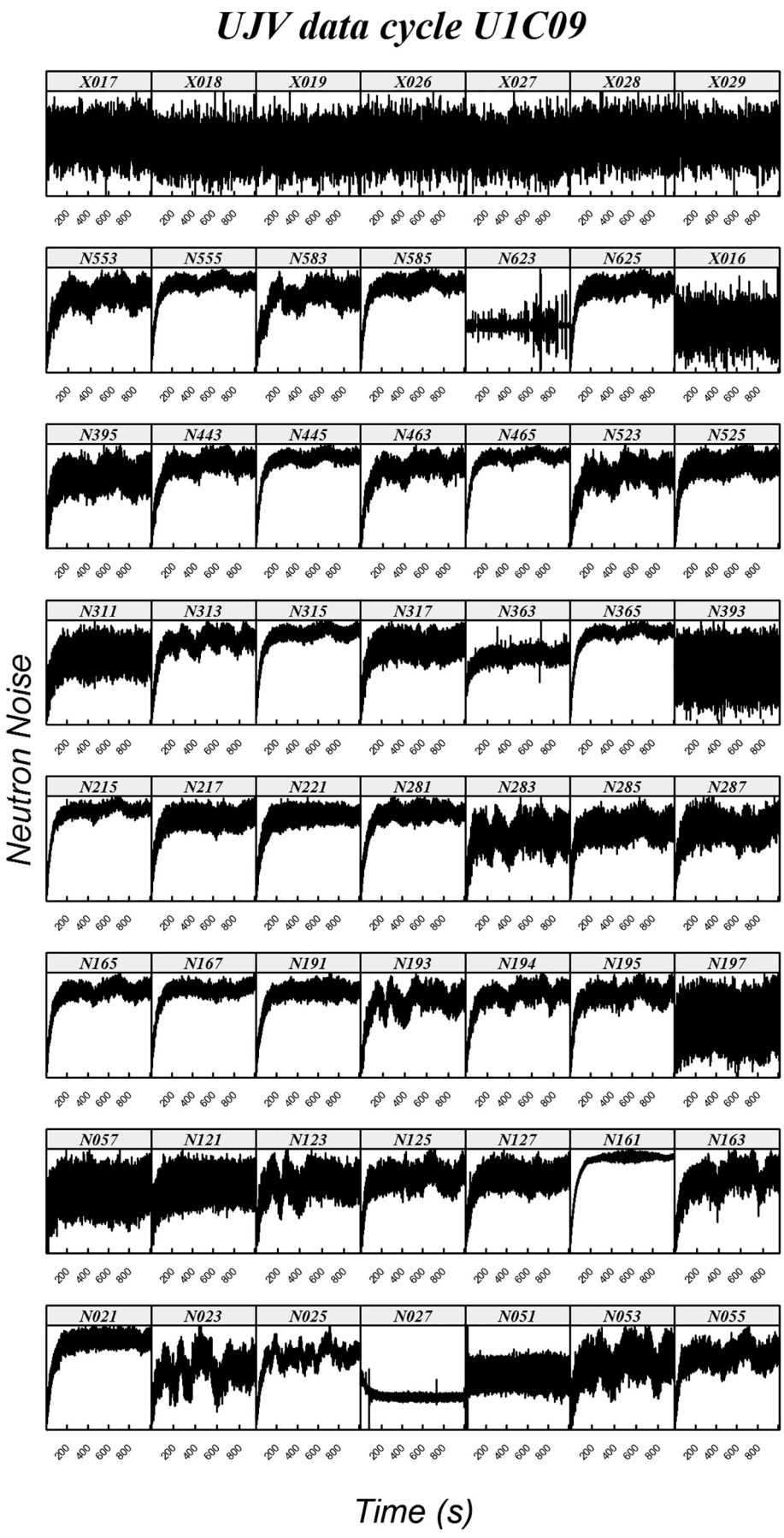

Fig. 18. Cycle U1-C09 overview in time domain of the ex-core detectors (first line) and the in-core detectors (the other lines).

estimated employing Welch's method and we compared the spectra by superposition in Fig. 27 with the same colours used in Fig. 26. The SSA improve the resolution of the spectrum. The SSA is able to extract two principal low frequencies (cf. Fig. 27) which could even be three frequencies according to the Fig. 29. We did a zoom of the spread frequencies of the welch periodogram around the frequency of 27 Hz (cf. Fig. 16 zoom-part-2) in Fig. 28 which gives some details on the separability of the classes. We only represented the classes 1,4,7,10 to facilitate the observation. The position of the classes can be observed in Fig. 26 with the same color code.

4.8. Discussion about the high number of frequencies highlighted by the SSA calculation

We use in this section a technic used in speech recognition. Thanks to the modelisation by an autoregressive model we assess resonance frequencies so-called formants (Snell and Milinazzo, 1993).

We can have an idea of the continuity in the presence of these formants during the cycle thanks to Fig. 30 which is the tracking of these formants detection by a sliding windows (512 points) on all the cycles. All the formants assessed by the autoregressive model

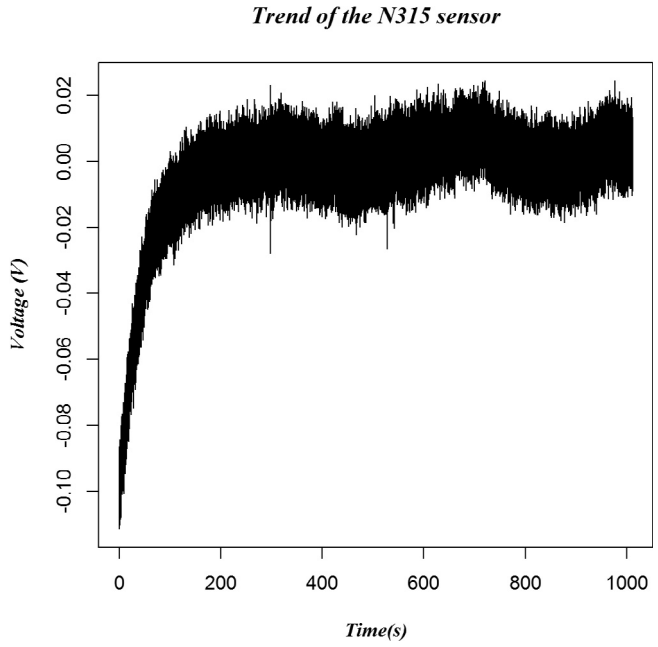

Fig. 19. Trend of the N315 in-core sensor.

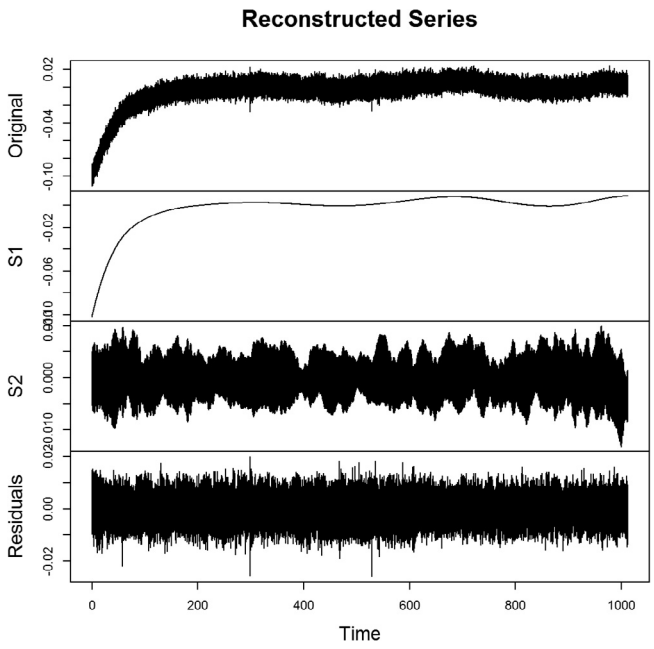

Fig. 21. Assessment of the trend by the SSA analysis.

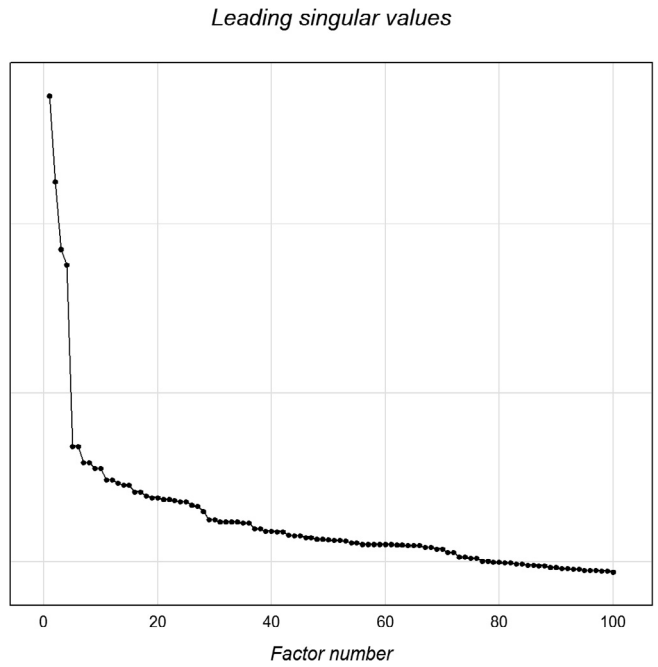

Fig. 20. SSA Eigen-values.

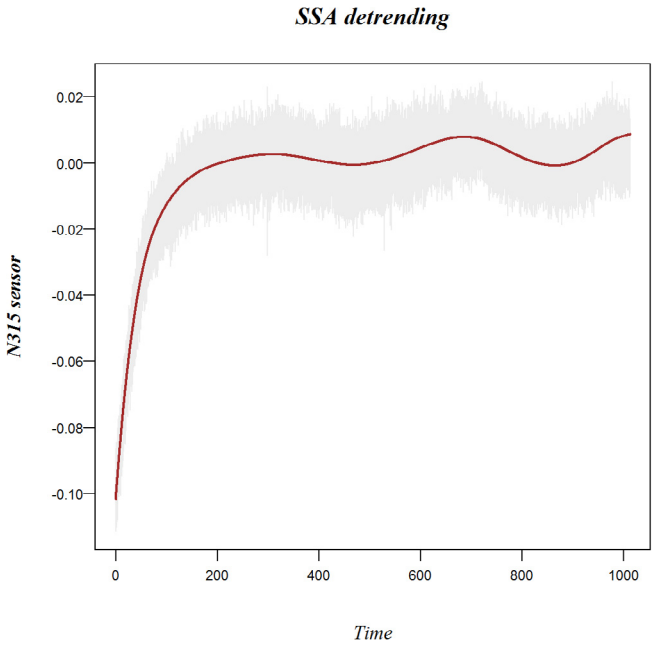

Fig. 22. SSA detrending.

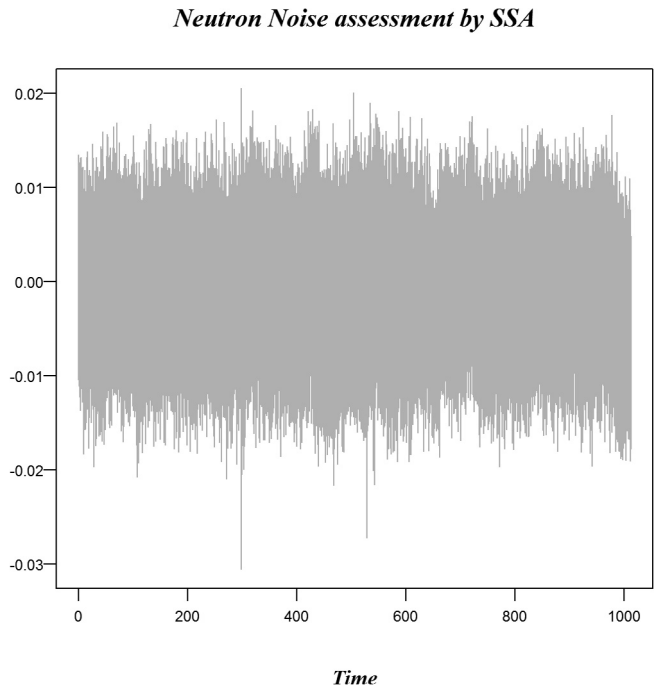

Fig. 23. SSA Neutron Noise assessment.

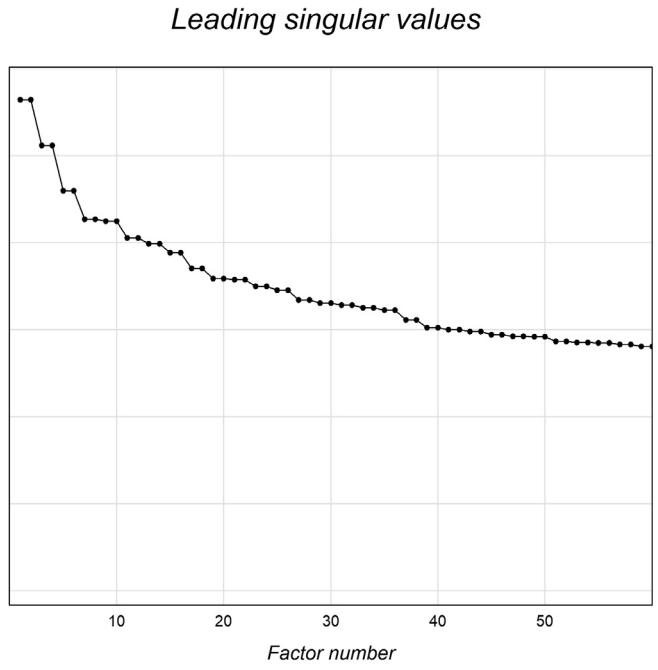

Fig. 24. Eigen values after detrending and filtering.

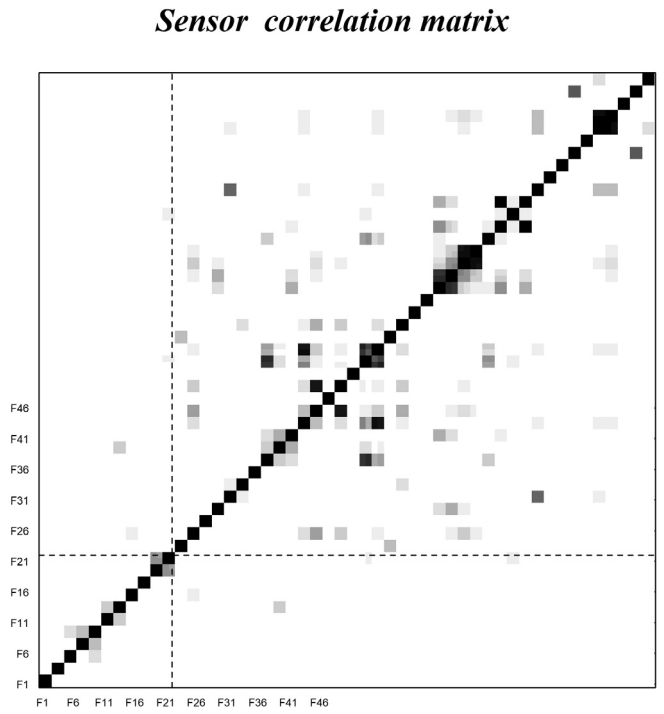

Fig. 25. Correlation matrix after detrending and filtering.

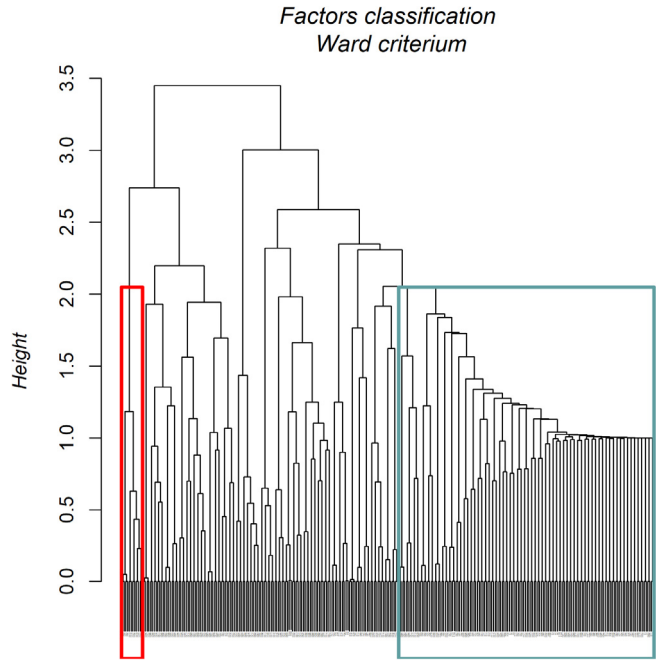

Fig. 26. Factors classification after detrending and filtering. We highlight only the class 1 (red) and 10 (green) for the understanding of the graph.

on the final spectrum are not always detected online. There is a strong variability. The medians of the online detected formants are reported in black dots lines on the welch PSD graph on the right side. Which is conspicious is the fact that only two formants are stable, the frequencies 24.34 and 33.21 Hz. Because of the shift between the median and the final formants (black and red dotted lines) we can deduce that all the phenomena linked to the other frequencies evolve during the cycle. On the contrary, these two stable frequencies must be linked to a physical phenomenon whose signature does not evolve during the cycle. On one hand, this observation can explain the frequential spreading observed in Fig. 16 (cf. part-2 and zoom-part-2) and on the other hand, certainly the significant amount of frequency identified by the SSA analysis.

We did not realized a quantitative analysis of the SSA concerning the spectral investigation. We only noticed on the results (cf. Figs. 27-28-29) that the spectral calculation carried out on the eigenvectors significantly improve the signal to noise ratio highlighting some specific frequencies comparing to the classic Welch calculation realized on the raw signal (cf. Fig. 30). We could even

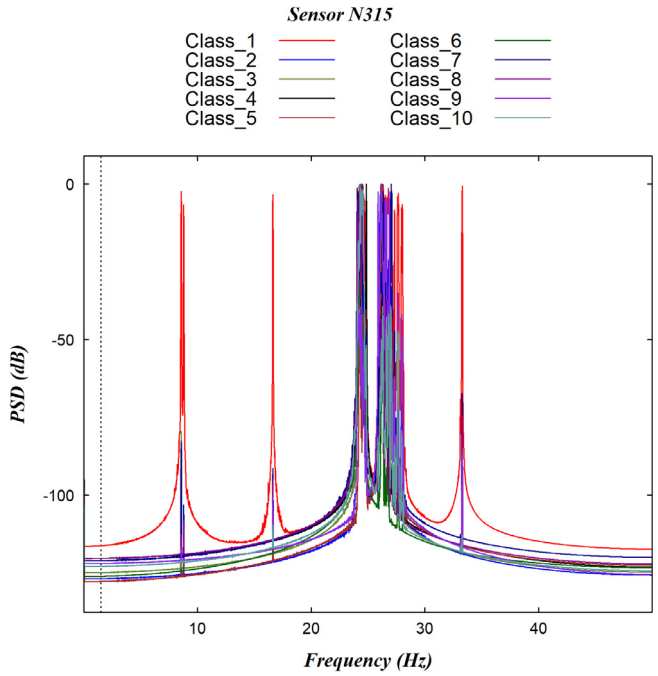

Fig. 27. Spectral decomposition after detrending and filtering.

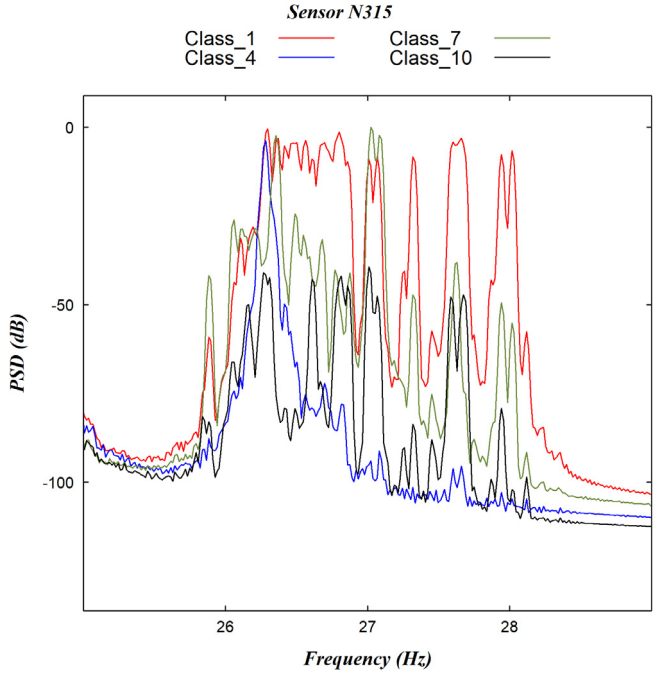

Fig. 28. Spectral decomposition after detrending and filtering - zoom on the middle frequencies.

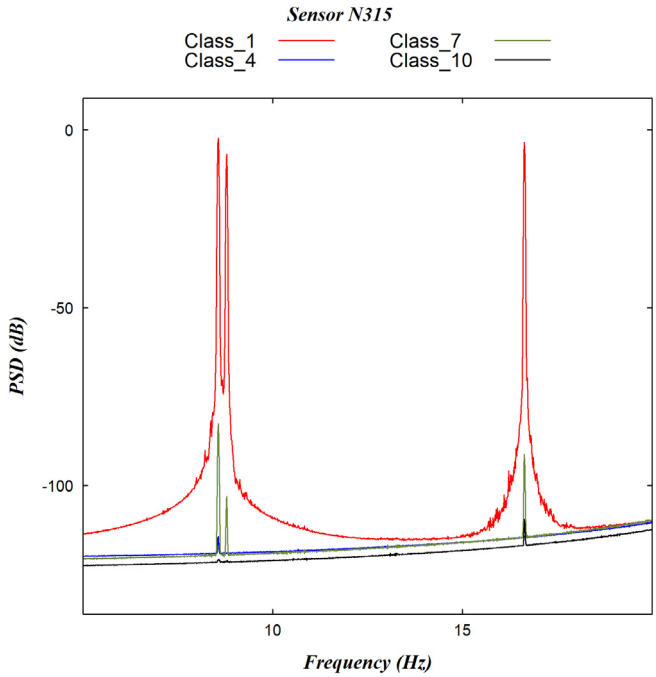

Fig. 29. Spectral decomposition after detrending and filtering - zoom on the low frequencies with the separation of two very close frequencies under 10 Hz.

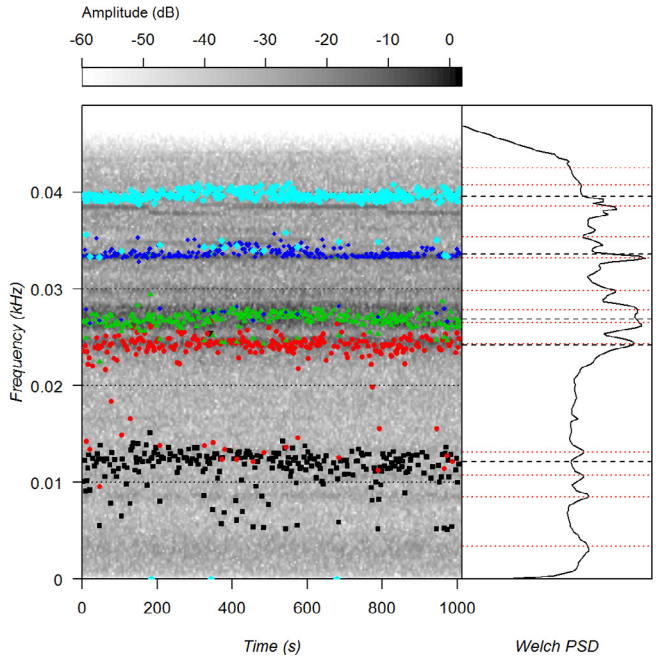

Fig. 30. Formants tracking.

separate two very close frequencies under 10 Hz (cf. Fig. 29). We did not use anymore these observations. We have to do further investigation in the relationship between Singular Spectrum Analysis and Fourier analysis (Bozzo et al., 2010) in order to be able to assess a better understanding of the highlighted frequencies by the SSA and get a robust physical interpretation pertained to the neutron noise phenomenon.

Eventually, in our case, the SSA was used mainly to remove the trend for each in-core signal which was an obligation before any further analysis. We removed the components linked to the trend during the reconstruction phase. We did not need a model and it works very well (cf. Figs. 22 and 23). The advantage of using SSA compared to a traditional Fourier analysis for this process is not to generate artifact (Rekapalli and Tiwari, 2016) in the output signal as with the classic filtering methods (as a delay introduction for example).

5. Operational modal analysis applied to neutron noise

The expression Operational Modal Analysis means the class of modal identification methods based on response measurements

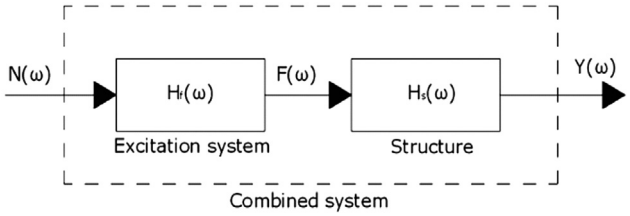

Fig. 31. Assumptions taken in Operational Modal Analysis techniques. Taken from (Rainieri and Fabbrocino, 2014).

only. It is widely used to characterize spectrum from accelerometers and displacement sensors for vibration monitoring in multiple applications such as aerospace, civil and industrial engineering (Eugeni et al., 2018,Gres et al., 2019,Rainieri and Fabbrocino, 2014).

One of the criteria for its application is the stationarity of the data analyzed and the assumption of certain hypothesis regarding the input. Thus, in the general case, the structure/system under study is assumed to be excited by unknown forces that are the output of the so-called excitation system loaded by white noise (see Fig. 31). Under this assumption, the measured response can be interpreted as the output of the combined system, made by the excitation system and the structure/system under test in series, to a stationary, zero mean, Gaussian white noise (Rainieri and Fabbrocino, 2014,Torres Delgado et al., 2021).

It has several advantages like its capability to deal with closely spaced resonances, to distinguish different sources of vibration that affect the spectrum in the same frequency range and to gather all the information from all the detectors available at different locations. In this respect, the method allows a multivariate approach and discriminating different spectral characteristics in the same frequency range by decomposing the spectra in different parts. Note that this type of discrimination in the same frequency range cannot be achieved by filtering with wavelets or Hilbert Huang Transform since these techniques decompose the signal into different frequency bands but they do not decompose the signal into different parts within the same frequency range.

Neutron noise is the result of different physical phenomena (Torres et al., 2019). For diagnostics purposes it is very important to distinguish which source is producing every spectral characteristic within the same frequency range. Standard noise analysis cannot distinguish this and in many occasions, a detailed characterization of the different sources affecting the neutron noise could answer many questions especially when certain changes have taken place in the plants. For instance, changes in fuel design that normally leads to changes in structural design, thermohydraulic parameters or others (Bermejo et al., 2017).

In general terms, modal analysis techniques provide the following info:

- Decomposed spectra that can give information of the different sources affecting the neutron noise.
- Characterization of the different resonances found in the decomposed spectra: amplitude, frequency and damping of every resonance.
- Spatial information of all the detectors and how every resonance is manifesting itself in each detector with both amplitude and phase.
- Distinguishing the different ranges of frequency depending on the spectral characteristics based on an objective criterion.

In the following subsections, some global results from the application of OMA are presented. First, an explanation of the steps to be followed to apply the methodology is described in subsection 5.1. In subsection 5.2, general results of the application of the methodology are presented as well as some focus on certain specific frequency ranges (subsection 5.2.15.2.1 and 5.2.2). At last, future lines of research are outlined.

5.1. Application of modal analysis: Enhanced frequency domain decomposition

Several methods are included under the term operational modal analysis. One of the most used is called Enhanced Frequency Domain Decomposition (EFDD). In this section, all the steps needed to apply this methodology are explained in detail:

1. Selecting the detectors to use in the analysis. In Operational Modal analysis, the detectors used are located on the structure under study so that they can monitor as best as possible all the vibrations. In the case of neutron noise, the in-core neutron detectors are the ones that comply with this criterion.

2. Construction of the PSD matrix ($G_{yy}(\omega)$) for each frequency step. The diagonal is composed of the APSD of each detector and the non-diagonals by the CPSDs. Its size is n $\times$ n where n is the number of detectors.

3. Singular value decomposition of the APSD matrix,

$$G_{yy} = U\Sigma U^H \tag{7}$$

where Σ is a diagonal matrix with the singular values in descending order. The U matrix contains the singular vectors which are the mode shapes $\{\phi_k\}$ at each frequency. The relationship between mode shapes and singular vectors can be found in (Rainieri and Fabbrocino, 2014). This decomposition leads to two different sources of information:

4. Singular values, which are used to construct the decomposed spectra. There will be as many decomposed spectra as number of detectors. Normally the first three singular values are the most important and the rest are negligible. Therefore, the dominant sources in neutron noise can be found in the first or second singular values.

5. Singular vectors, which give information on the phase of every single detector at every frequency step and in the different decomposed spectra.

Thus, for a certain frequency step, there are n singular values and for every singular value, there is a singular vector whose coordinates give information on how the spectrum is manifesting itself in each detector. Let us say that the singular value is the amplitude, and the singular vector gives the phase in each detector at that particular frequency.

6. Modal assurance criterion (MAC) (Pastor et al., 2012). It is the criterion used to determine the frequency range of the resonance under study.

$$MAC = \frac{\left|\{\phi_{ref}\}^H\{\phi_k\}\right|^2}{\left(\{\phi_{ref}\}^H\{\phi_{ref}\}\right)\left(\{\phi_k\}^H\{\phi_k\}\right)} \tag{8}$$

where $\{\phi_{ref}\}$ is the singular vector (mode shape) at the peak of the resonance and $\{\phi_k\}$ is a singular vector around the vicinity of a resonance. Normally, as a general rule (Rainieri and Fabbrocino, 2014, Pastor et al., 2012), the threshold value of 0.8 is used to consider the similarity between two mode shapes.

7. Obtaining the parameters of the resonances under study: amplitude, frequency and damping. Firstly, the inverse Fourier transform of the singular value spectra gives the autocorrelation function which lead to the frequency and the damping ratio of the resonance. For more details, see (Montalvo et al., 2021).

8. Characterize certain frequency ranges. For neutron noise diagnostics, obtaining the resonances of every decomposed spectrum may not be useful. Sometimes, a preliminary approach based

on studying the singular values and the singular vectors phases can give a lot of information to the plants on the type of phenomena affecting neutron noise.

5.2. Examples of application in real plant data

In this section, some examples of the application of EFDD in real plant data will be described. The data used for this analysis belong to two KWU reactors: a three loop and a four loop. In the first case, the in-core detectors are located in six radial positions and in six axial levels, making a total of 36 detectors. In the second case, there are 48 in-core detectors located in eight radial positions and six axial levels. The figures presented in this section belong to the second case, as it has more detectors and it is more suitable to exemplify the application of the methodology. The results of both reactors have not been included since it would be redundant. At the end of this section, comments on the results observed on the three-loop reactor will be also included.

In Fig. 32, there is an example of the decomposed spectra after applying the singular value decomposition in the four loop reactor. The decomposition has been performed by using all the in-core detectors. The graph shows the first five singular values (SVDi). As can be seen the first three singular values are the most important, whereas the fourth and fifth in purple and green colors respectively, present very low values. Note that the decomposed spectra gather all the information from all detectors included in the analysis. Therefore, the spectra from the first singular values contains the dominant sources that affect the neutron noise at every frequency.

Apart from the singular values, the singular vectors give information on the phase relationship between all the detectors at every frequency range. In the next subsection, an example of the representation of the singular vector phases will be shown.

When there is a need to focus on a particular frequency band, it is important to use the MAC to determine the frequency range of interest. For instance, if the interest is characterizing the peak around 1 Hz, the MAC should be calculated for every decomposed spectra following equation (2). As can be seen in Fig. 33 on the left, the MAC is calculated for SVD1-SVD3. The region of interest is determined for MAC values above 0.8. In the right subfigure, the frequency range obtained for every SVD is established. The Peak around 1 Hz is present in SVD1 and its frequency range goes from 0.8 to 1.6 Hz according to MAC. Following the steps of EFDD, amplitude, frequency and damping of that resonance could be calculated. In SVD2, the peak around 1 Hz is not present but there is another one at around 0.6 Hz. As can be seen, these two closely spaced resonances can be separated with this methodology and properly monitored in time for diagnostics purposes.

5.2.1. Beam mode range

In order to see the possibilities of the EFDD, we will explore some of the results obtained with this methodology. In Westinghouse reactors, in the beam mode region (7–8 Hz), opposite neutron detectors present out of phase (Pázsit et al., 2016). Nevertheless, in KWU reactors, in this region there is an in phase relationship between all detectors. Some authors have indicated that this is due to a pressure wave or fluid resonance (Runkel, 1987,Viebach et al., 2018). In fact, when EFDD is applied to the 4 loop reactor, all detectors present the same phase as can be seen in the phase of the first singular vector in Fig. 34. For the second singular vector, out of phase is observed. It is very likely that in this frequency region, the neutron noise is affected by different sources.

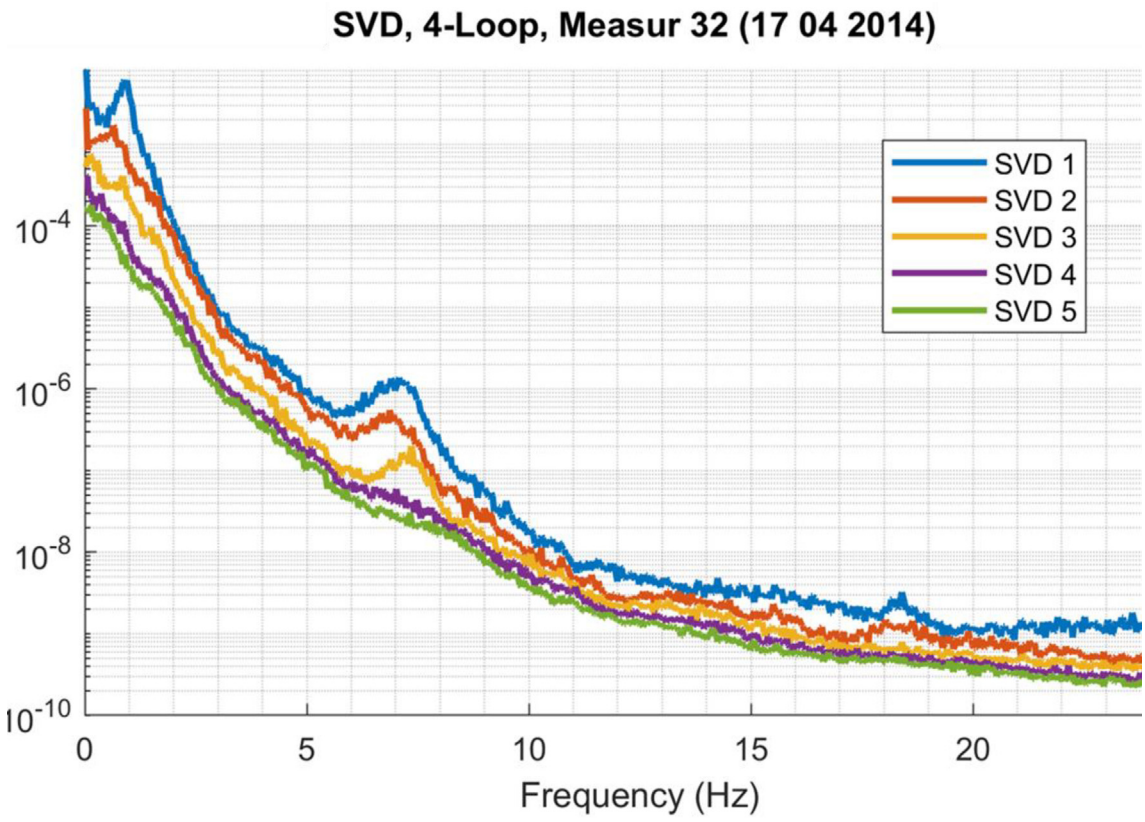

Fig. 32. Singular values spectra for the in-core detectors in the four-loop KWU.

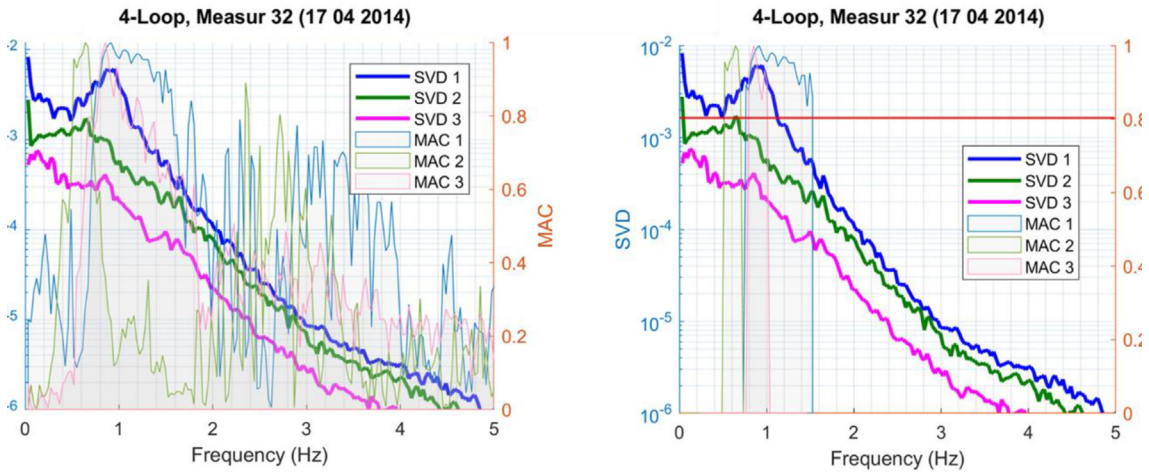

Fig. 33. SVD spectra and MAC values for the 4 loop in-core neutron detectors data in the frequency range below 2 Hz in the left subfigure. In the right subfigure, same info plus the MAC 0.8 threshold value is added as a red line.

The first singular value and vector may be due to the pressure wave and the second singular value/vector may be the consequence of a pendular motion.

In order to see this in 3D, Fig. 35 shows the phase of the first singular vector at every detector location in the vicinity of 7.5 Hz. As can be observed, all detectors present approximately the same phase, between 150 and 180 degrees.

The phase of the second singular vector can be seen in Fig. 36. Note that certain detectors present out of phase between each other. On one hand, there are strings like J02, J06, O05, G10, N12 and G14 that present 180° phase, whereas certain detectors from strings C04 and B12 present zero phase, that is they are out of phase with respect to the rest of the detectors (J02, J06, O05, G10, N12 and G14). It is possible that the pendular motion is

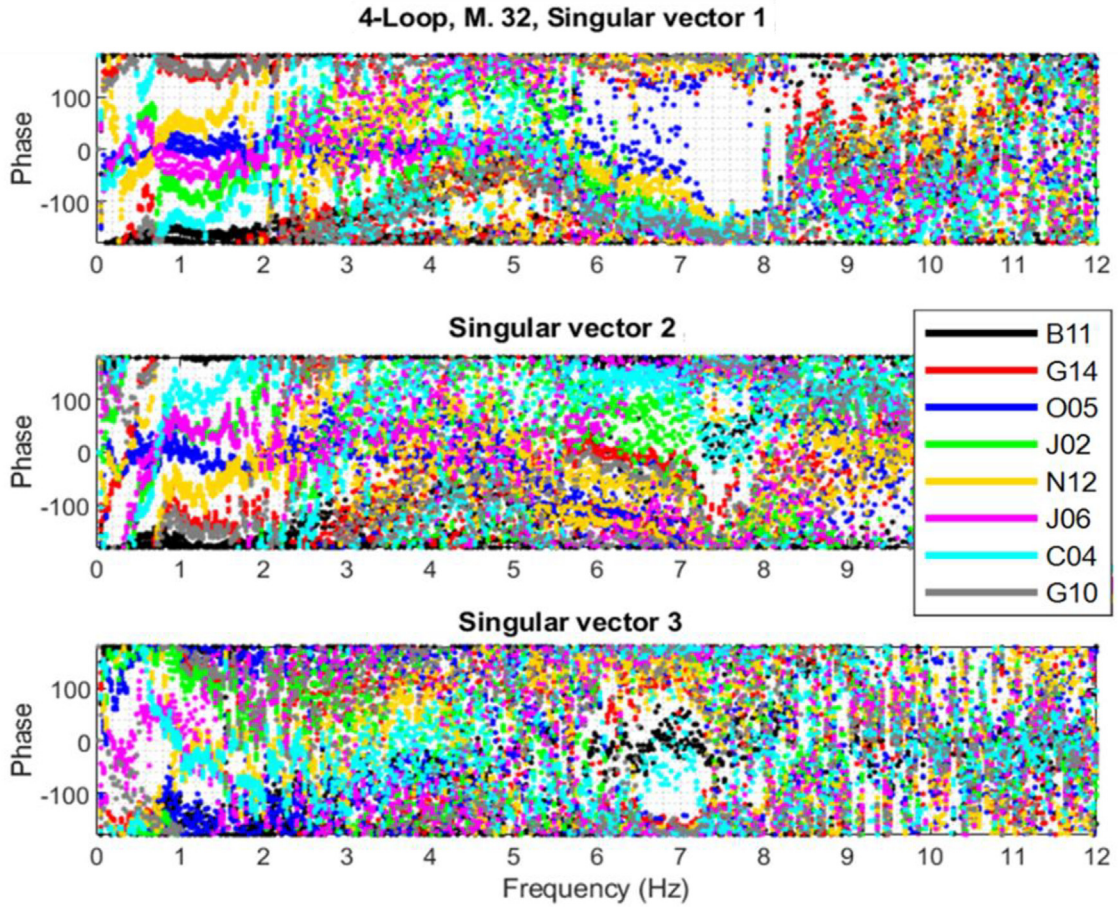

Fig. 34. Phases of the singular vectors in every in-core neutron detector for the four-loop KWU reactor.

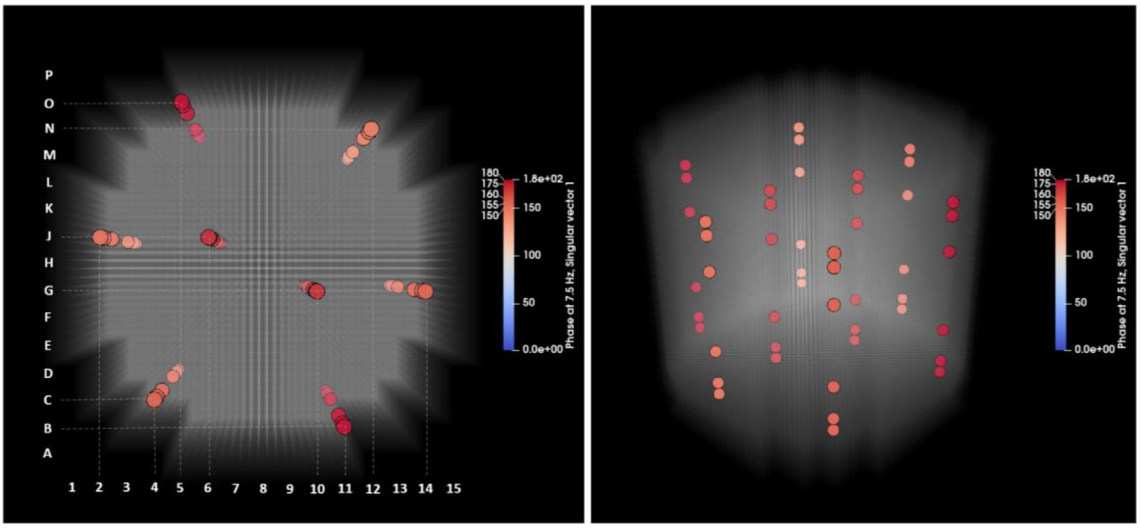

Fig. 35. Phases of the first singular vector at 7.5 Hz in the four loop KWU reactor.

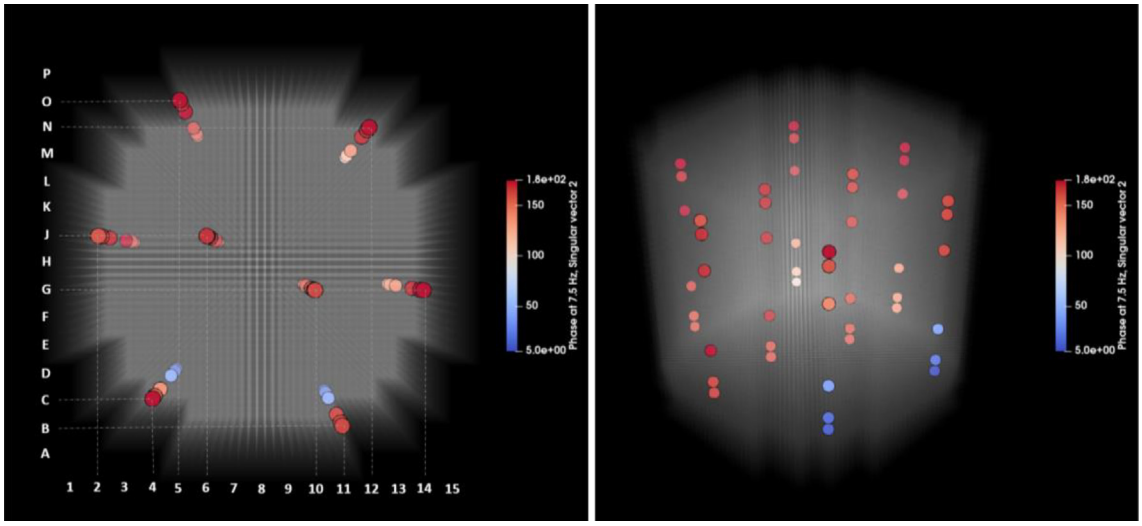

Fig. 36. Phases of the second singular vector at 7.5 Hz in the four loop KWU reactor.

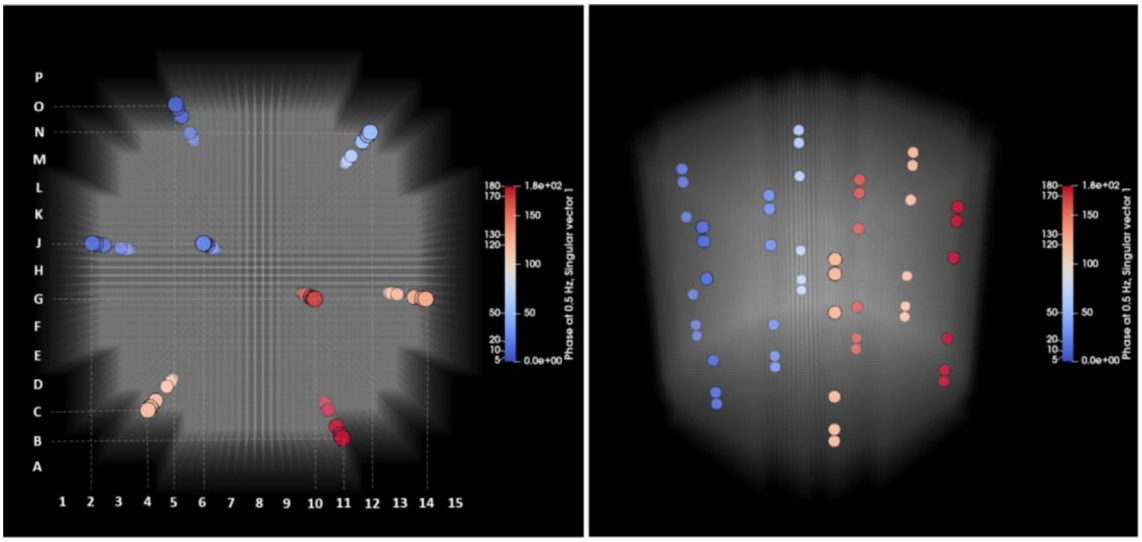

Fig. 37. Phases of the first singular vector at 0.5 Hz in the four loop KWU reactor.

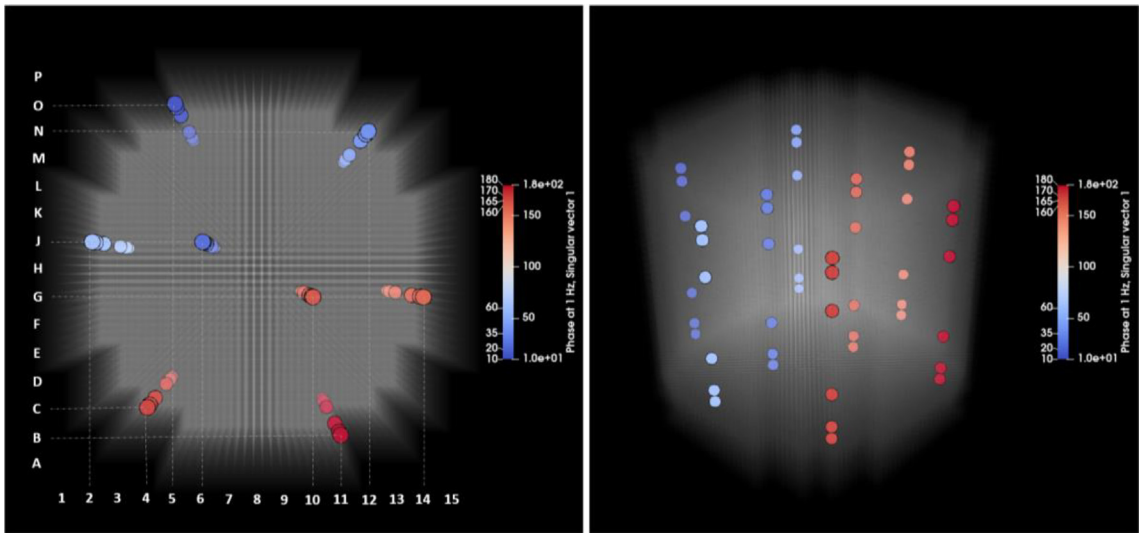

Fig. 38. Phases of the first singular vector at 1 Hz in the four loop KWU reactor.

manifesting in this second singular value/vector since the out of phase is observed among the detectors.

5.2.2. Low frequency range (1 Hz)

In the low frequency range, apart from the in phase behavior between detectors in the same string, which is something that has been previously observed by noise analysis (Seidl et al., 2015), it is possible to see an out of phase behaviour between detectors located in opposite halves of the reactor at 0.5 Hz (Fig. 37) and at 1 Hz (Fig. 38). This has also been observed in other reactors as can be seen in (Hashemian, 2009), where spectral characteristics like this were linked to a flow shifting phenomenon.

It is important to mention that in both reactors, three-loop and four loop, the singular value decomposition was very similar between each other. The singular value spectra for the three loop reactor has a profile very similar to the one presented in Fig. 33, where two resonances are observed: the one in the thermohydraulic range and the one in the beam mode range. Regarding the distribution of phases of the first singular vectors, the behavior is almost the same in both reactors. Therefore, presenting figures for the three loop reactor would be redundant. The results of the four loop reactor, as it has more detectors, (48 instead of 36) allow to illustrate better the capabilities of the methodology to deal with a high number of time series simultaneously. This is one of the main advantages of OMA. Naturally, the resonances of each reactor have particular values for amplitude, damping and frequency. The detailed study of these parameters for each reactor and its comparison constitute a possible future line of research.

As can be seen, the possibilities of OMA are numerous: from obtaining closely spaced resonances to identifying different sources of neutron noise, as well as 2D and 3D visualization of the results. In order to take advantage as much as possible of its possibilities, it should be supported by simulation efforts and feedback from the plants.

Future lines involving use of OMA techniques in KWU should focus on characterizing resonances in different frequency ranges, monitoring of these results, full characterization of the low frequency range, use of the decomposed spectra for the optimization of monitoring capabilities, etc.

6. Conclusions

In this work, several signal processing methods have been applied to plant data within the framework of the EU project COR-TEX. The data analyzed come from four different reactors: two KWU reactors and two VVER reactors.

Coolant velocities were estimated by evaluating three VVER-440 measurements and the results were verified with inserting them into the trend of standard evaluations. Narrower transit time peaks of the impulse response functions were demonstrated with comparing them with cross correlation functions at different levels of background noise.

The article showed how the Singular Spectral Analysis can be used to deeply analyze the neutron noise signal in the time domain following the following phases:

- phase 1: signal decomposition in order to identify and analyze its different components
- phase 2: obtain the spectrum of the different components
- phase 3: classification of these components according to their frequency content
- phase 4: signal reconstruction as the sum of those components of interest. We can then remove the components we are not interested in: trend, certain harmonics, noise.

After revealing the different spectral components of the signal, we are able to assess the value of the frequencies with a better resolution than that appearing in the welch periodograms. Now, we have to analyze these results according to physical investigation in order to explain the highlighted frequencies. In order to adjust the degree of precision, we can launch again the analysis asking for further investigation. The analysis has been carried out in such a way to generate a reproducible document automating the data processing thanks to the literate programming approach in the framework of the R language (Xie, 2021). Thus, we will be able to investigate different periodograms smooths, SSA decomposition (number of eigen vectors) and reconstruction (results of factor classifications).

Enhanced Frequency Domain Decomposition is a method inside the Operational Modal Analysis methodology that is able to analyze all the detectors in the core simultaneously. It decomposes the signal from all the detectors in the frequency domain in the so called Singular Value Decomposed spectra which represent different sources of perturbation in the data. Every decomposed spectra can be deeply characterized by means of the modal assurance criterion (MAC), which divides the spectra into frequency ranges of equal modal characteristics. Those frequency ranges can be studied in detail by different means. The results show that the

3D plots with the phase of each perturbation in every detector are very useful for monitoring purposes and for identifying different types of phenomena.

As a general conclusion, all the methods applied are used to distinguish different sources of perturbation that can be tracked in the neutron detectors. The standard traditional noise Fourier based methods struggle to extract certain components of the signals with high resolution. In the cases proposed, the characterization of the neutron detectors frequency content is improved by applying decomposition techniques in the frequency or in the time domain. Besides, in the case of OMA methodology, the decomposition is multivariate, so the results gather all the spectral information from all the detectors in the reactor.

The article gives an overview of the possibilities of each methodology. Nevertheless, more research is needed jointly with the plants and the simulation groups to fully identify the different harmonics and decomposed signals and spectra extracted with these methods. The link between the spectral characteristics found and the physical phenomena behind them needs to be further investigated for every reactor.

Declaration of Competing Interest

The authors declare that they have no known competing financial interests or personal relationships that could have appeared to influence the work reported in this paper.

Acknowledgements

The research leading to these results has received funding from the Euratom research and training programme 2014-2018 under grant agreement No 754316 (Project CORTEX Core Monitoring Techniques Experimental Validation and Demonstration).

References

Adorján, F., Czibók, T., Kiss, S., Krinizs, K., Végh, J., 2000. Core asymmetry evaluation using static measurements and neutron noise analysis. Ann. Nucl. Energy 27 (7), 649–658.
Bermejo, J.A., Montalvo, C., Ortego, A., 2017. On the possible effects contributing to neutron noise variations in KWU-PWR reactor: Modelling with S3K. Prog. Nuclear Energy 95, 1–7.
Bermejo, J.A., 2014. Neutron flux noise calculations with Simulate- 3K. I. Studsvik International Core Management Software Users Group Meeting.
Blázquez, J., Montalvo, C., García-Berrocal, A., Balbás, M., 2013. Searching the beginning of BWR power instability events with the Hilbert Huang transform. Ann. Nucl. Energy 54, 281–288.
Bozzo, E., Carniel, R., Fasino, D., 2010. Relationship between Singular Spectrum Analysis and Fourier analysis: Theory and application to the monitoring of volcanic activity. Comput. Math. Appl. 60 (3), 812–820.
Broomhead, D.S., Jones, R., King, G.P., Pike, E.R., 2020. Singular system analysis with application to dynamical systems. In: Anonymous Chaos, Noise and Fractals. CRC Press, pp. 15–27.
Chionis, D., Dokhane, A., Ferroukhi, H., Girardin, G., Pautz, A., 2018. Noise Phenomenology: Part I – Simulation of Stochastic Phenomena with Simulate-3K. PHYSOR 2018: Reactor Physics paving the way towards more efficient systems Cancun, Mexico , 1001.
Demazière, C., 2020. The CORTEX project: Improving nuclear fleet operational availability. Nuclear News.
Dokhane, A., Mylonakis, A., 2018. Description of simulated data, Deliverable. CORTEX.
Eugeni, M., Coppotelli, G., Mastroddi, F., Gaudenzi, P., Muller, S., Troclet, B., 2018. OMA analysis of a launcher under operational conditions with time-varying properties. CEAS Space Journal 10 (3), 381–406.
Golyandina, N., Nekrutkin, V., Zhigljavsky, A.A., 2001. Analysis of Time Series Structure: SSA and Related Techniques. CRC Press.
Gres, S., Andersen, P., Damkilde, L., 2019. Operational Modal Analysis of Rotating Machinery, in Anonymous Rotating Machinery, Vibro-Acoustics & Laser Vibrometry, Volume 7. Springer, 67–75.
Hashemian, H., 2009. On-Line Monitoring Applications in Nuclear Power Plants.
Hashemian, H.M., 2011. On-line monitoring applications in nuclear power plants. Prog. Nuclear Energy 53 (2), 167–181.
Hassani, H., 2007. Singular spectrum analysis: methodology and comparison.
Kantz, H., Schreiber, T. (Eds.), 2004. Nonlinear Time Series Analysis. Cambridge University Press.
Kiss, S., Lipcsei, S., 2019. Method for Coolant Velocity Estimation in the Reactor Core Using In-Core SPND Detectors. Proceedings of the International Conference Nuclear Energy for New Europe, Portorož, Slovenia, September 9–12, 2019. Nuclear Society of Slovenia, pp. 1010.1–1010.14. https://arhiv.djs.si/nene2019/proceedings/index.html.
Kiss, S., Lipcsei, S., 2022. Analysis and enhancements of the coolant velocity estimation method in PWR core. Annals of Nuclear Energy 174. https://doi.org/10.1016/j.anucene.2022.109146.
Montalvo, C., García-Berrocal, A., Bermejo, J.A., Queral, C., 2014. Advanced surveillance of Resistance Temperature Detectors in Nuclear Power Plants. Ann. Nucl. Energy 65, 35–40.
Montalvo, C., Gavilán-Moreno, C.J., García-Berrocal, A., 2017. Cofrentes nuclear power plant instability analysis using ensemble empirical mode decomposition (EEMD). Ann. Nucl. Energy 101, 390–396.
Montalvo, C., Pázsit, I., Nylén, H., Dykin, V., 2016. First evidence of the pivotal motion ("Tilting Mode") of the Core Barrel in the Ringhals-4 PWR. Physics of Reactors. PHYSOR 2016 , Physics of Reactors. PHYSOR 2016.
Montalvo, C., Torres, L.A., García-Berrocal, A., 2021. Beam mode characterization by applying operational modal analysis to neutron detectors data. Nucl. Eng. Des. 385, 111503.
Pantera, L., Traore, O.I., 2015. Reproducible data processing research for the CABRI RIA experiments acoustic emission signal analysis. , 1-8.
Pastor, M., Binda, M., Harčarik, T., 2012. Modal assurance criterion. Procedia Engineering 48, 543–548.
Pázsit, I., Montalvo, C., Tran, H.N., Nylén, H., Guerrero, O.O., 2017. Ringhals Diagnostics and Monitoring. Ann. Res. Rep., 2016–2017
Pázsit, I., Nylén, H., Montalvo-Martin, C., 2014. Refined method for surveillance and diagnostics of the core barrel vibrations of the Ringhals PWRs. Physor 2014 , Physor 2014.
Pázsit, I., Torres, L.A., Montalvo, C., Nagy, L., Szieberth, M., Klujber, G., Misawa, T., Kitamura, Y., Nylén, H., 2019. Ringhals diagnostics and monitoring. Ann. Res. Rep., 2019–2020
Pázsit, I., Montalvo, C., Nylén, H., Andersson, T., Hernández-Solís, A., Cartemo, P.B., 2016. Developments in core-barrel motion monitoring and applications to the ringhals PWR Units. Nucl. Sci. Eng. 182 (2), 213–227.
Prieto-Guerrero, A., Espinosa-Paredes, G., 2014. Decay Ratio estimation in boiling water reactors based on the empirical mode decomposition and the Hilbert-Huang transform. Prog. Nucl. Energy 71, 122–133.
Rainieri, C., Fabbrocino, G., 2014. Operational modal analysis of civil engineering structures. Springer New York, New York, NY.
Rekapalli, R., Tiwari, R.K., 2016. Singular spectral analysis based filtering of seismic signal using new Weighted Eigen Spectrogram. J. Appl. Geophys. 132, 33–37.
Runkel, J., 1987. Noise Analysis in Pressurized Water Reactor. PHD Thesis .
Seidl, M., Kosowski, K., Schüler, U., Belblidia, L., 2015. Review of the historic neutron noise behavior in German KWU built PWRs. Prog. Nuclear Energy 85, 668–675.
Snell, R.C., Milinazzo, F., 1993. Formant location from LPC analysis data. IEEE Trans. Speech Audio Process. 1, 129–134.
Stulík, P., Bem, M., Tschiesche, J., Machek, J., 2019. WP4 progress report on subtask T4.2.3, CORTEX project.
Stulík, P., et al., 2019. Development of advanced signal processing techniques and evaluation results, CORTEX Project.
Tagaris, T., Ioannou, G., Sdraka, M., Alexandridis, G., Stafylopatis, A., 2019. Putting Together Wavelet-Based Scaleograms and Convolutional Neural Networks for Anomaly Detection in Nuclear Reactors. , 237-243.
The European CORTEX project, 2018. The European CORTEX project.
Torres Delgado, L.A., Verma, V., Montalvo, C., Dokhane, A., García-Berrocal, A., 2021. Operational modal analysis for characterization of mechanical and thermal–hydraulic fluctuations in simulated neutron noise. Nucl. Eng. Des. 373, 111017.
Torres, L.A., Chionis, D., Montalvo, C., Dokhane, A., García-Berrocal, A., 2019. Neutron noise analysis of simulated mechanical and thermal-hydraulic perturbations in a PWR core. Ann. Nucl. Energy 126, 242–252.
Traore, O.I., Favretto-Cristini, N., Pantera, L., Cristini, P., Viguier-Pla, S., Vieu, P., 2017a. Which methods and strategies to cope with noise complexity for an effective interpretation of acoustic emission signals in noisy nuclear environment? Acta Acustica United with Acustica 103 (6), 903–916.
Traore, O.I., Pantera, L., Favretto-Cristini, N., Cristini, P., Viguier-Pla, S., Vieu, P., 2017b. Structure analysis and denoising using singular spectrum analysis: application to acoustic emission signals from nuclear safety experiments. Measurement 104, 78–88.
Traore, O., Pantera, L., Favretto-Christini, N., Viguier-Pla, S., 2016. Emission acoustique et traitement du bruit: cas de signaux expérimentaux en contexte nucléaire.
Viebach, M., Bernt, N., Lange, C., Hennig, D., Hurtado, A., 2018. On the influence of dynamical fuel assembly deflections on the neutron noise level. Prog. Nuclear Energy 104, 32–46.
Xie, Y, 2021. Knitr: A General-Purpose package for dynamic report generation in R. CRC Press.